iScience

CellPress
OPEN ACCESS

Article

Endofin is required for HD-PTP and ESCRT-0 interdependent endosomal sorting of ubiquitinated transmembrane cargoes

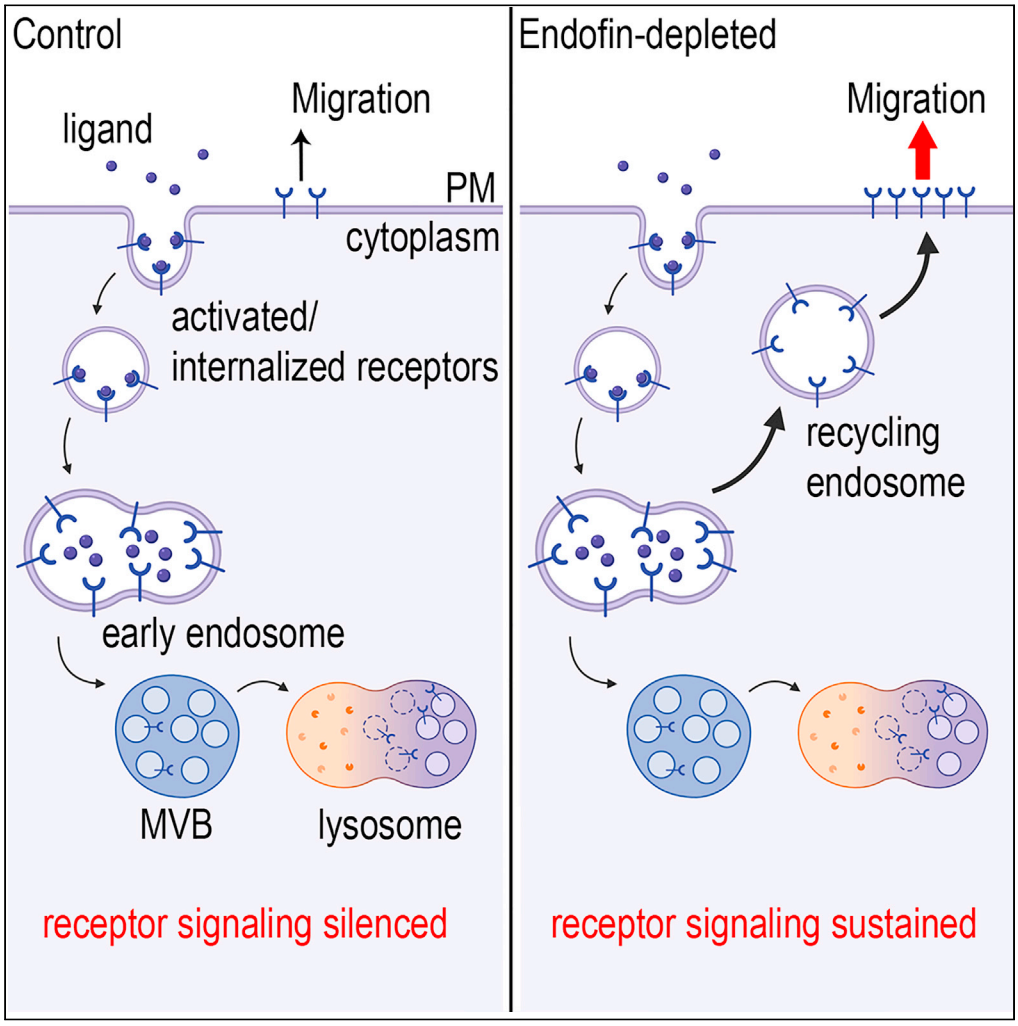

Jalal M. Kazan, Guillaume Desrochers, Claire E. Martin, ..., Anne-Claude Gingras, Gergely L. Lukacs, Arnim Pause

gergely.lukacs@mcgill.ca (G.L.L.)
arnim.pause@mcgill.ca (A.P.)

Highlights

Endofin forms a complex with ESCRT proteins and EGFR on early endosomes

Endofin is required for activated EGFR and integrin α5 lysosomal targeting

Endofin promotes HD-PTP colocalization with ESCRT-0 and -III on early endosomes

Endofin depletion increases cell migration and sustains receptor signaling

Kazan et al., iScience 24, 103274
November 19, 2021
https://doi.org/10.1016/j.isci.2021.103274

iScience

CellPress
OPEN ACCESS

Article

Endofin is required for HD-PTP and ESCRT-0 interdependent endosomal sorting of ubiquitinated transmembrane cargoes

Jalal M. Kazan,[1,2,6] Guillaume Desrochers,[1,2,6] Claire E. Martin,[3] Hyeonju Jeong,[1,2] Dmitri Kharitidi,[1,2] Pirjo M. Apaja,[5] Ariel Roldan,[5] Nicole St. Denis,[3] Anne-Claude Gingras,[3,4] Gergely L. Lukacs,[2,5,7,*] and Arnim Pause[1,2,7,8,*]

SUMMARY

Internalized and ubiquitinated signaling receptors are silenced by their intraluminal budding into multivesicular bodies aided by the endosomal sorting complexes required for transport (ESCRT) machinery. HD-PTP, an ESCRT protein, forms complexes with ESCRT-0, -I and -III proteins, and binds to Endofin, a FYVE-domain protein confined to endosomes with poorly understood roles. Using proximity biotinylation, we showed that Endofin forms a complex with ESCRT constituents and Endofin depletion increased integrin α5-and EGF-receptor plasma membrane density and stability by hampering their lysosomal delivery. This coincided with sustained receptor signaling and increased cell migration. Complementation of Endofin- or HD-PTP-depleted cells with wild-type Endofin or HD-PTP, but not with mutants harboring impaired Endofin/HD-PTP association or cytosolic Endofin, restored EGFR lysosomal delivery. Endofin also promoted Hrs indirect interaction with HD-PTP. Jointly, our results indicate that Endofin is required for HD-PTP and ESCRT-0 interdependent sorting of ubiquitinated transmembrane cargoes to ensure efficient receptor desensitization and lysosomal delivery.

INTRODUCTION

Receptor signaling is a tightly regulated cellular process. Ligand-activated receptors are endocytosed and internalized to the endosomal compartments where they remain an active signaling hub (Sorkin and von Zastrow, 2009). At the endosomal surface, transmembrane cargo segregation into different microdomains by different machineries determines cargo fate; sorting toward tubulovesicular recycling or toward lysosomal degradation (Norris et al., 2017). Receptor resensitization takes place when receptors are recycled back to the plasma membrane (PM). Alternatively, signal termination occurs when receptors are targeted for lysosomal degradation. Receptor downregulation is initiated by their sorting and incorporation into intraluminal vesicles (ILVs) to form the multivesicular bodies (MVBs). This process is accomplished by the endosomal sorting complexes required for transport (ESCRT) machinery.

The ESCRT machinery is composed of five protein complexes responsible for the formation of an ILV. ESCRT-0, -I and -II proteins are recruited to the endosomal membranes and directly interact with multi-mono- or poly-ubiquitinated receptors. ESCRT-III proteins mediate membrane deformation and scission whereas the Vps4 complex is responsible for ESCRT-III disassembly and their recycling back to the cytoplasm (Christ et al., 2017; Vietri et al., 2020). The MVBs will then fuse to the lysosomes and their cargo will be degraded or exocytosed. By controlling the fate of numerous receptors, ESCRT proteins are crucial regulators of cell signaling events underlying key cellular processes such as cell migration and proliferation (Kharitidi et al., 2015; Miller et al., 2018; Szymanska et al., 2018; Toyoshima et al., 2007), as well as in the elimination of misfolded or damaged PM proteins (Okiyoneda et al., 2010).

Likewise, clathrin is associated with ESCRTs playing a key role in both cargo concentration and ILV formation (Wenzel et al., 2018; Raiborg et al., 2001, 2006). It is recruited to early endosomes by the ESCRT-0 protein Hrs (Raiborg et al., 2001, 2006). Static and live cell imaging of the prototype epidermal growth factor

[1]Goodman Cancer Research Center, McGill University, Montreal, QC H3A 1A3, Canada

[2]Biochemistry Department, McGill University, Montreal, QC H3G 1Y6, Canada

[3]Lunenfeld-Tanenbaum Research Institute, Sinai Health System, Toronto, ON M5G 1X5, Canada

[4]Department of Molecular Genetics, University of Toronto, Toronto, ON M5S 1A8, Canada

[5]Physiology Department, McGill University, Montreal, QC H3G 1Y6, Canada

[6]These authors contributed equally

[7]Senior author

[8]Lead contact

*Correspondence: gergely.lukacs@mcgill.ca (G.L.L.), arnim.pause@mcgill.ca (A.P.)

https://doi.org/10.1016/j.isci.2021.103274

receptor (EGFR) indicated that the initial steps of ILV formation consist of a wave of ESCRT-0, ESCRT-I, clathrin, and HD-PTP recruitment (Wenzel et al., 2018).

The ESCRT protein HD-PTP (*PTPN23*) was shown to affect the degradation of ubiquitinated receptors such as TGFβ/BMP receptors, PDGFRβ, EGFR, integrins, neurotrophin, and EphB2 receptors (Ali et al., 2013; Doyotte et al., 2008; Kharitidi et al., 2015; Ma et al., 2015; Miller et al., 2018; Stefani et al., 2011; Budzinska et al., 2020; Lahaie et al., 2019). HD-PTP directly binds to ESCRT-0, -I and -III proteins and contributes to the endosomal sorting of ubiquitinated receptors toward MVBs and lysosomal degradation (Ali et al., 2013; Doyotte et al., 2008; Gahloth et al., 2016, 2017b; Ichioka et al., 2007; Kharitidi et al., 2015). During the early phase of ILV formation, recruitment of ESCRT-0, -I and HD-PTP increase until ESCRT-III is recruited, after which they begin dissociating from the endosomal membrane (Wenzel et al., 2018). HD-PTP also acts as a tumor suppressor and its haploinsufficiency was shown to increase cell migration and invasion (Manteghi et al., 2016). Rescue experiments further demonstrated that the N-terminus of HD-PTP, containing the Bro1 and V domain, was sufficient to restore most of the EGFR trafficking defects observed upon HD-PTP depletion (Doyotte et al., 2008). This minimal functional unit of HD-PTP indeed retains the capacity to bind ubiquitinated cargo as well as several components of the ESCRT machinery such as STAM2 (ESCRT-0) and CHMP4B (ESCRT-III) (Desrochers et al., 2019; Gahloth et al., 2016, 2017b; Lee et al., 2016; Pashkova et al., 2013). Interestingly, the same region of HD-PTP which binds STAM2 and CHMP4B was also shown to bind Endofin (*ZFYVE16*) (Gahloth et al., 2017b).

Endofin is a large protein composed of a central FYVE domain enabling its proper localization to the membrane of early endosomes where it can form a complex with receptors such as TGFβR1 (Chen et al., 2007a). It also displays a Smad binding domain next to its FYVE domain and was found to impact TGFβ and BMP signaling (Chen et al., 2007a; Goh et al., 2015; Shi et al., 2007). Furthermore, the C-terminus of Endofin directly interacts with Tom1, a protein that binds to clathrin and ubiquitinated receptors (Seet et al., 2004; Yamakami et al., 2003). Endofin was shown to recruit clathrin to early endosomes via its direct interaction with Tom1 (Seet and Hong, 2005). However, the impact and significance of Endofin-mediated clathrin recruitment on ubiquitinated cargo trafficking is still poorly understood.

Endofin binds HD-PTP with higher affinity than STAM2 and CHMP4B (Gahloth et al., 2017a, 2017b). The competition between ESCRT proteins for HD-PTP binding was, therefore, proposed to interfere with the capacity of the receptor to engage with ESCRT components and to be efficiently delivered to the lysosomes (Gahloth et al., 2017a; Lee et al., 2016). The direct interaction between Endofin and HD-PTP also suggests a broader role for Endofin in ESCRT-dependent receptor trafficking and signaling, as well as in ubiquitinated membrane cargo sorting in general.

Here, we show that Endofin is required for the ESCRT-dependent lysosomal sorting of integrin α5, EGFR and other poly-ubiquitinated transmembrane model cargo. We propose that Endofin is permissive for HD-PTP interaction and colocalization with ESCRT-0 and facilitates clathrin recruitment to early endosomes. Thus, disruption of Endofin binding to HD-PTP is sufficient to severely compromise ESCRT-mediated lysosomal ubiquitinated-cargo sorting. Consequently, Endofin depletion caused sustained receptor signaling and increased cell migration. Altogether, this study identifies Endofin as a key regulator of ESCRT-dependent receptor trafficking and cell signaling.

RESULTS

Endofin forms a complex with ESCRTs and EGF receptor

Endofin directly binds Tom1 and HD-PTP, both of which have direct roles in receptor trafficking (Doyotte et al., 2008; Gahloth et al., 2017a; Katoh et al., 2004; Kharitidi et al., 2015; Seet et al., 2004; Yamakami et al., 2003). Endofin's interactome is likely to reflect its function; however, it remains poorly characterized. To investigate the binding partners of HD-PTP and Endofin in further detail, two proteomic workflows were designed. In the first, we performed proximity-dependent biotin tagging (BioID), in which a biotin ligase (BirA*) fused to the N- or C-terminus of either HD-PTP and Endofin are used as 'baits' to covalently tag nearby proteins ('preys') with biotin, which can then be purified and identified by MS (Lambert et al., 2015). Subsequently, an affinity-purification mass spectrometry (AP-MS) approach was employed, with an inducible expression of Flag-tagged HD-PTP and Endofin as baits. Our findings reveal Endofin as a robust proximity interactor of HD-PTP by BioID and AP-MS (Figures 1A and S1B), and that HD-PTP forms a complex with a variety of ESCRT proteins from different ESCRT complexes (ESCRT-0, -I and -III)

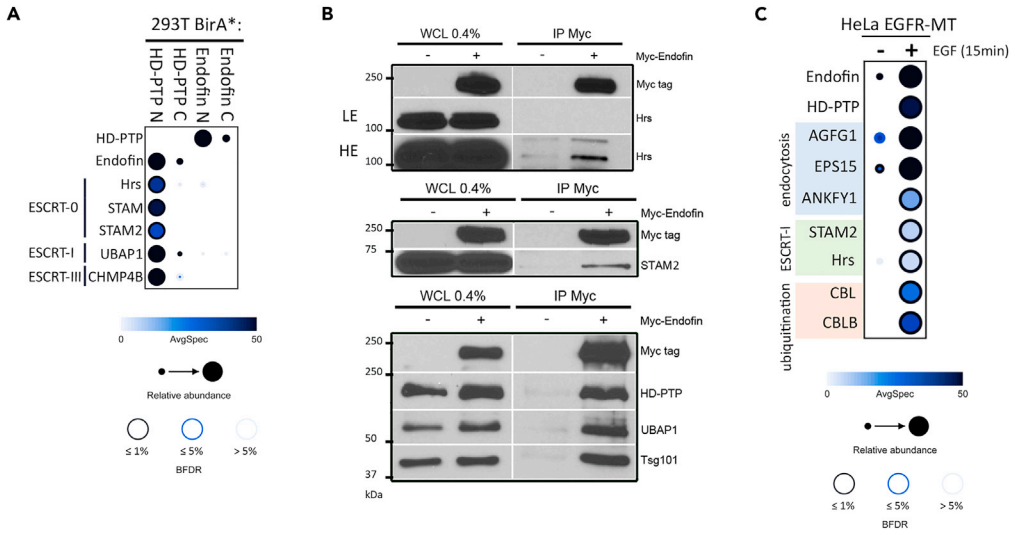

Figure 1. Endofin forms a complex with ESCRTs and EGF receptor

(A) Dot plot of BioID screen showing ESCRT proteins in close proximity to HD-PTP and Endofin. Flag-tagged biotin ligase (BirA*) was fused to the N- or C-terminus of HD-PTP and Endofin and were used as baits. Constructs were transfected into Flp-In T-REx 293T cells. Fill shades in the dot plot indicate the average spectral counts (Avg Spec), the size of the dot represents its relative abundance across all preys and the outer circle color represents the BFDR value.

(B) Co-immunoprecipitation (co-IP) performed on 293T cells transiently transfected with myc-Endofin compared to mock transfected cells. Myc-Endofin was immunoprecipitated (myc antibody) and co-IP of HD-PTP, ESCRT-0 (Hrs and STAM2) and ESCRT-I (Tsg101 and UBAP1) were assessed by Western blots. Whole cell lysate (WCL) is loaded to reveal protein content. Low exposure (LE) and high exposure (HE) immunoblots are shown for Hrs. Data are from n = 3 independent experiments.

(C) Dot plot of TurboID screen showing ESCRT proteins and other proteins related to endocytosis and EGFR activation in close proximity to EGFR in the presence or absence of EGF stimulation (100 ng/mL, 15 min). Fast-acting miniTurbo biotin ligase (MT) was fused to the C-terminus of EGFR (EGFR-MT) and transfected into Flp-In T-REx HeLa cells and used as bait.

(Figure 1A). Likewise, HD-PTP was identified as a proximity interactor of Endofin-BirA* (Figure 1A), and while interactions between Endofin and ESCRT proteins were not detected by BioID (Figure 1A), AP-MS revealed that various ESCRT proteins (HD-PTP, ESCRT-I and -III) complex with Endofin (Figure S1B). Further, our results demonstrate HD-PTP as a robust interactor of clathrin heavy chain 1 (CLTC) and, more broadly, endocytic and trafficking machinery within the cell (Figure S1B). Collectively, these proteomic assays demonstrate that Endofin and HD-PTP form a complex with endocytic machinery and ESCRTs (further annotated in Figure S1A). To better understand the role of Endofin in relation to HD-PTP, BioID data were further analyzed using the STRING database, by which networks of interaction were designed and clustered into different cellular processes. In support of our observations, Endofin's network is linked to receptor trafficking, a finding that paralleled that of HD-PTP (Figures S2 and S3) (Doyotte et al., 2008).

To validate that Endofin, HD-PTP, and ESCRTs are forming a complex on early endosomes, isopycnic sucrose gradient centrifugation was performed on 293T cell organelles. While Endofin and HD-PTP were absent in cellular fractions containing LAMP1 and Tom20, the lysosome and mitochondria markers, respectively (Figure S1C), they were present together within cellular fractions containing ESCRT proteins (Hrs, Tsg101, and UBAP1). Tom1 and the early endosomal marker EEA1 were also present in these fractions. In addition, subcellular fractionation followed by size-exclusion chromatography (HPLC) showed Endofin, HD-PTP and ESCRT-0 components (Hrs and STAM2) as part of large protein complexes ranging from 525 to 927 kDa, however the ESCRT-I component Tsg101 was found mostly within complexes of lower molecular weight (Figure S1D). As a further validation of complex formation with ESCRT proteins, co-immunoprecipitation was performed on transiently expressed myc-Endofin. Indeed, Endofin showed to form a complex with HD-PTP, ESCRT-0 (Hrs and STAM2) and ESCRT-I (Tsg101 and UBAP1) (Figure 1B), where STAM2, Tsg101, and UBAP1 directly interact with HD-PTP (Ali et al., 2013; Gahloth et al., 2016; Ichioka et al., 2007). This data further supports that Endofin is part of a complex containing HD-PTP and ESCRTs on early endosomes.

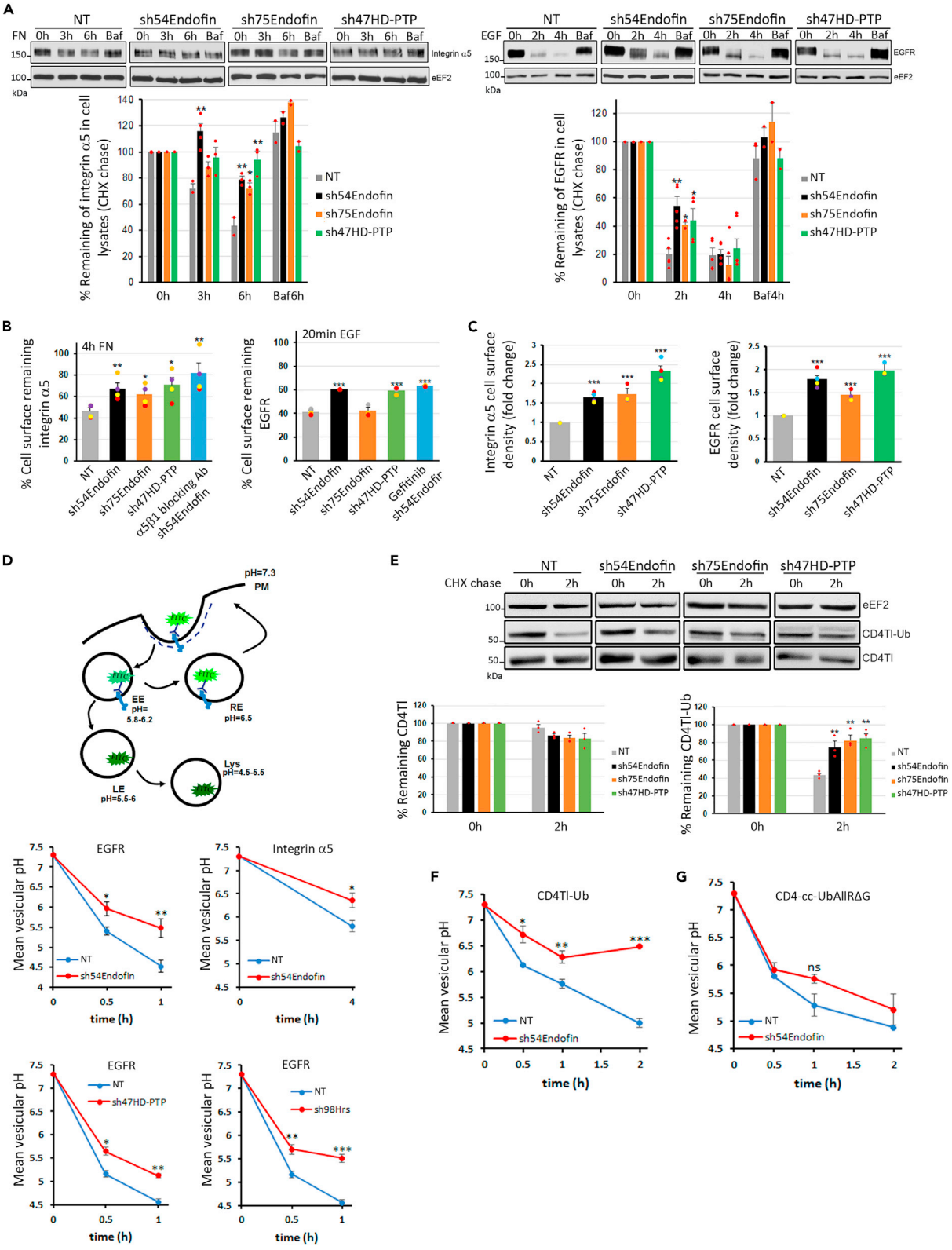
A
NT
sh54Endofin
sh75Endofin
sh47HD-PTP
FN
0h 3h 6h Baf
Integrin α5
eEF2
kDa
% Remaining of integrin α5 in cell lysates (CHX chase)
0h 3h 6h Baf6h
EGF
0h 2h 4h Baf
EGFR
% Remaining of EGFR in cell lysates (CHX chase)
0h 2h 4h Baf4h
B
4h FN
% Cell surface remaining integrin α5
α5β1 blocking Ab
20min EGF
% Cell surface remaining EGFR
Gefitinib
C
Integrin α5 cell surface density (fold change)
EGFR cell surface density (fold change)
D
pH=7.3
PM
EE
pH= 5.8-6.2
RE
pH=6.5
Lys
pH=4.5-5.5
LE
pH=5.5-6
EGFR
Integrin α5
Mean vesicular pH
time (h)
sh98Hrs
E
CHX chase
CD4TI-Ub
CD4TI
% Remaining CD4TI
% Remaining CD4TI-Ub
F
CD4TI-Ub
G
CD4-cc-UbAIIRΔG
ns

Figure 2. Endofin mediates the efficient sorting of integrin α5, EGFR and CD4 poly-ubiquitinated cargo model toward lysosomal degradation

(A) Integrin α5 (left panel) and EGFR (right panel) cycloheximide chase (10 μg/mL CHX) of total receptor levels in Endofin- and HD-PTP-depleted HeLa cells. Cells were serum-starved (2 h), pre-treated with CHX (1 h) and then receptors were activated either with fibronectin (10 μg/mL FN, 37°C) or with EGF (50 ng/mL, 37°C). Integrin α5 was chased for 0, 3 and 6 h, whereas EGFR was chased for 0, 2 and 4 h in the presence of CHX. Control cells were also pre-treated with Bafilomycin A1 (200 nM Baf + CHX, 1 h) to inhibit lysosomal acidification and hence lysosomal degradation (6 h FN + Baf or 4 h EGF + Baf). Western blots were performed on cell extracts to measure degradation kinetics by densitometric analysis using ImageJ software. Integrin α5 and EGFR levels were normalized to eEF2.

(B) Integrin α5 (left panel) and EGFR (right panel) plasma membrane (PM) stability in HeLa cells measured by cell surface-ELISA (cs-ELISA). After serum starvation, receptors were activated either with fibronectin (10 μg/mL FN, 4 h, 37°C) or with EGF (50 ng/mL, 20 min, 37°C). α5β1 integrin blocking antibody (10 μg/mL) and Gefitinib (2 μM) were used as negative controls to block receptor internalization in Endofin-depleted cells. For each cell line, levels of integrin α5 and EGFR are plotted as percentage remaining at the cell surface compared to unstimulated cells.

(C) cs-ELISA was performed on serum-starved HeLa cells to quantify integrin α5 (left panel) and EGFR (right panel) PM receptor density at steady states. Endofin- and HD-PTP-depleted cells are compared to control NT cells.

(D) (upper panel) Schematic representation of changes in vesicular pH during receptor trafficking (EE: early endosomes, RE: recycling endosomes, LE: late endosomes, Lys: lysosomes). (Lower panel) FRIA analysis of EGFR and integrin α5 endocytosis kinetics in serum-starved HeLa cells. Mean vesicular pH of FITC-labeled EGFR- or integrin α5-containing endocytic vesicles determined by FRIA in Endofin-, HD-PTP- and Hrs-depleted HeLa cells compared to NT cells. After serum starvation, cells were either stimulated with EGF (50 ng/mL, 30 or 60 min, 37°C) or with FN (10 μg/mL, 4 h, 37°C).

(E) Endofin- and HD-PTP-depleted 293T cells were transiently transfected with CD4TI (negative control for receptor sorting toward lysosomal degradation) or with CD4TI-Ubiquitin chimera (CD4TI-Ub, which serves as a model for poly-ubiquitinated cargo). Serum-starved 293T cells were pre-treated with CHX (100 μg/mL) to chase total protein levels of CD4TI and CD4TI-Ub for 2 h. Western blots (CD4 antibody) were performed on cell extracts to measure degradation kinetics by densitometric analysis using ImageJ software. CD4TI and CD4TI-Ub levels were normalized to eEF2.

(F and G) (F) Mean vesicular pH of CD4TI-Ub- and (G) CD4TCC-UbAllRΔG-containing endocytic vesicles determined by FRIA in Endofin-depleted HeLa cells compared to NT cells after 15-, 30-, 60- and 120-min chase (37°C). CD4TCC-UbAllRΔG serves as a model for tetrameric mono-ubiquitinated cargo. Data are mean ± SEM of n ≥ 3 independent experiments. Unpaired student t-test: *p < 0.05, **p < 0.01, ***p < 0.001.

Finally, we probed whether EGFR activation elicits Endofin recruitment using MiniTurbo BioID, which allows for shortened labeling time as compared to the BirA* enzyme. Results showed that upon EGF stimulation Endofin and HD-PTP are rapidly recruited to EGFR along with common endocytic machineries (Figure 1C). Altogether, this data demonstrates that Endofin forms a complex with HD-PTP, ESCRTs, and EGFR, suggesting that Endofin might have a role in regulating receptor trafficking.

Endofin regulates plasma membrane density, stability, and lysosomal degradation of integrin α5 and EGFR

HD-PTP is known to have a direct role in regulating EGFR, integrin α5, and PDGFRβ endo-lysosomal membrane trafficking (Belle et al., 2015; Doyotte et al., 2008; Kharitidi et al., 2015). Since Endofin directly interacts with HD-PTP and forms a complex with different ESCRTs (Gahloth et al., 2017b) and EGFR, we thought to investigate the role of Endofin in receptor trafficking. We used HD-PTP-depleted HeLa cells as a positive control to disrupt receptor trafficking (Figure S4A). HeLa cells were Endofin-depleted by shRNA and infected with a non-target shRNA (NT) as a negative control for depletion (Figure S4A). Western blotting of total cell lysates from Endofin- and HD-PTP-depleted cells revealed at least 2.5-fold increase in cellular expression levels of integrin α5 (Figure S4B), and ∼1.2–1.6-fold increase in EGFR levels (Figure S4C).

Several studies have demonstrated that ligand activation, ubiquitination, and internalization of both integrin α5 and EGFR facilitate their sorting toward lysosomal degradation (Alwan et al., 2003; Kharitidi et al., 2015; Lobert et al., 2010). Next, we assessed the effect of Endofin depletion on integrin α5 and EGFR lysosomal degradation kinetics in comparison to HD-PTP depletion. Serum-starved cells were stimulated with fibronectin (3 and 6 h) or EGF (2 and 4 h) in the presence of cycloheximide (CHX) to inhibit protein synthesis. To inhibit lysosomal degradation, cells were pretreated with Bafilomycin A1 (1 h) in the presence of CHX. Western blots revealed that upon Endofin and HD-PTP depletion, lysosomal degradation of integrin α5 and EGFR was delayed by >60% and ∼40% after 6 and 2 h chase, respectively (Figure 2A), suggesting that Endofin plays a role in integrin α5 and EGFR lysosomal degradation.

Considering the crosstalk between ESCRT and ubiquitinated transmembrane proteins, which are preferentially targeted toward lysosomal degradation over recycling back to the PM, we asked whether Endofin depletion can delay the PM turnover of activated receptors. Cell surface stability of activated integrin α5 and EGFR were measured by cell surface ELISA (cs-ELISA) upon fibronectin (4 h) and EGF (20 min) stimulation, respectively. Compared to NT cells, ∼ 20% of integrin α5 was stabilized at the PM resembling the effect of an integrin α5β1 blocking antibody, which interferes with the activation and internalization of the receptor (Figure 2B). Similarly, ∼ 20% of EGFR was stabilized at the PM upon Endofin depletion.

A comparable effect was shown for Gefitinib, an EGFR inhibitor that blocks receptor activation, ubiquitination, and internalization (Figure 2B). Notably, Endofin and HD-PTP depletion had no effect on the internalization rate of EGFR upon EGF stimulation (5 min) (Figure S4D). Moreover, using cs-ELISA we measured steady state PM receptor density upon Endofin and HD-PTP depletion. Integrin α5 and EGFR cell surface densities increased by at least 1.5-fold compared to NT cells (Figure 2C). Thus, Endofin depletion likely delays the lysosomal degradation of both integrin α5 and EGFR and increases their PM density and stability by facilitating recycling at the early endosome level.

Endofin is required for the efficient lysosomal delivery of integrin α5 and EGFR

If the lysosomal degradation of integrin α5 and EGFR is delayed upon Endofin depletion, it is plausible that Endofin has a role in ESCRT-dependent receptor sorting from early endosomes toward MVBs and lysosomes. Hence, to better understand the role of Endofin in the endo-lysosomal transfer kinetics, receptor delivery to lysosomes was determined by monitoring the pH of receptor-containing vesicles (pH_v) by fluorescent ratiometric image analysis (FRIA) (Figure 2D) (Barriere and Lukacs, 2008). HD-PTP- and Hrs-depleted HeLa cells (Figure S4A) were used as positive controls for the disruption of receptor trafficking (Kharitidi et al., 2015; Wenzel et al., 2018). First, serum-starved cells were labeled on ice with anti-EGFR or anti-integrin α5 followed by $F(ab')_2$ secondary antibody coupled to the pH-sensitive fluorescein isothiocyanate (FITC). Next, to induce synchronized receptor internalization, cells were stimulated with EGF (30- and 60-min chase, 37°C) or with fibronectin (4 h chase, 37°C) and pH_v was measured by FRIA. As expected, EGFR trafficking was delayed after a 30- and 60-min chase in HD-PTP- and Hrs-depleted cells ($pH_v \sim 5.7 \pm 0.09$ and $pH_v \sim 5.7 \pm 0.1$, respectively) compared to NT cells ($pH_v \sim 5.2 \pm 0.07$) (Figures 2D and S4E). Strikingly, after 30 min EGFR chase in Endofin-depleted cells, the receptor is confined to early endosomes ($pH_v \sim 6 \pm 0.17$), however, in NT cells EGFR is delivered to late endosomes ($pH_v \sim 5.4 \pm 0.07$) (Figures 2D and S4E). In addition, after 60 min chase, EGFR is delivered to late endosomes in Endofin-depleted cells ($pH_v \sim 5.4 \pm 0.23$), whereas in NT cells EGFR is delivered to lysosomes ($pH_v \sim 4.5 \pm 0.1$) (Figures 2D and S4E). Endofin depletion also inhibited the egress of integrin α5 from early endosomes ($pH_v \sim 6.4 \pm 0.1$) while in control NT cells the receptor was delivered to late endosomes ($pH_v \sim 5.7 \pm 0.1$) (Figure 2D). The FRIA results clearly demonstrate that Endofin has a crucial role in the transport of receptors from early endosomes toward MVBs and lysosomes. This is exemplified by the identical effects of HD-PTP and Hrs depletion on EGFR trafficking.

Endofin is required for the efficient lysosomal delivery of poly-ubiquitinated model cargo

The recognition of ubiquitinated receptors by ESCRTs is a key step in the sorting process of internalized receptors toward MVBs and lysosomes. To examine whether Endofin also contributes to the endo-lysosomal sorting of ubiquitinated cargoes incapable of receptor signaling, we used the established CD4-Ub chimera which undergoes constitutive poly-ubiquitination. For this, two different model receptors were used. One was truncated CD4 (CD4TI), in which the cytoplasmic tail was deleted and replaced with a linker, thus lacking a ubiquitin acceptor site and sorting signal (Barriere et al., 2006). In addition, we used CD4TI-Ub, a chimera where the linker has been fused to a ubiquitin (Ub) moiety. The fusion of a single Ub moiety to the linker is sufficient to induce constitutive poly-ubiquitination of the CD4TI-Ub, which in turn accelerates its ESCRT-dependent lysosomal delivery (Apaja et al., 2010; Barriere et al., 2007).

Endofin- and HD-PTP-depleted cells were transiently transfected with CD4TI and CD4TI-Ub constructs to assess their degradation kinetics by CHX chase (2 h). Western blotting demonstrated that the lysosomal degradation of ~40% CD4TI-Ub was delayed upon Endofin and HD-PTP depletion compared to NT cells (Figure 2E). As expected, Endofin and HD-PTP depletion had no significant effect on the levels of CD4TI (Figure 2E). Furthermore, FRIA showed that Endofin depletion confined CD4TI-Ub to recycling endosomes ($pH_v \sim 6.4 \pm 0.07$) compared with NT cells where it is delivered to lysosomes ($pH_v \sim 4.8 \pm 0.07$) after a 2-h chase (Figure 2F). Hence, Endofin is required for the efficient lysosomal degradation of poly-ubiquitinated cargoes, even in the absence of second messenger signaling activity. To assess whether Endofin-dependent endo-lysosomal sorting has a preference toward specific ubiquitinated cargo, lysosomal delivery of the tetrameric mono-ubiquitinated cargo (CD4TCC-UbAllRΔG) was also determined by FRIA upon Endofin depletion. In CD4TCC-UbAllRΔG, a tetramerization signal was inserted before the Ub moiety and all seven Lys residues of the Ub moiety were replaced with Arg and the carboxy-terminal Gly residues were deleted (Barriere et al., 2006). Consistent with the effect of HD-PTP depletion on CD4TCC-UbAllRΔG trafficking (Kharitidi et al., 2015), Endofin depletion did not affect the trafficking of the tetrameric mono-ubiquitinated cargo (Figure 2G), even though it was previously shown that the tetrameric mono-ubiquitin can serve as an

efficient endocytic signal (Barriere et al., 2006). These data show that Endofin does not only play a role in EGFR and integrin α5 trafficking, but it regulates the specific sorting of poly-ubiquitinated cargo toward lysosomal degradation.

Endofin depletion decreases clathrin recruitment to early endosomes

Endofin recruits clathrin via Tom1 to early endosomes (Seet and Hong, 2005), and Tom1 directly interacts with Endofin and with clathrin heavy chain (Seet and Hong, 2005; Seet et al., 2004) (Figure S5C). Our data demonstrates that clathrin colocalization with EGFR reached a peak (~0.65 ± 0.09) after a 15-min EGFR chase (Figures S5A and S5B). To better understand why receptor trafficking is delayed upon Endofin depletion, we first assessed the effect of Endofin depletion on clathrin recruitment to early endosomes by immunofluorescence. Endofin-depleted HeLa cells were transiently transfected with Rab5Q79L, a GTPase deficient mutant, to induce the formation of enlarged endosomes (Raiborg et al., 2001; Wegener et al., 2010). Upon Endofin depletion, clathrin recruitment decreased by 33% ± 3% compared to NT cells (Figures S5D and S5E). In addition, we assessed Tom1 interaction with clathrin heavy chain in Endofin-depleted cells, and co-IP showed that clathrin interaction with Tom1 decreased upon Endofin depletion (Figure S5F). Since clathrin is indispensable for receptor clustering on the endosomal surface and their accumulation in ILVs during MVB biogenesis (Wenzel et al., 2018), this might contribute to the delay in EGFR lysosomal delivery. To mimic the recruitment of Tom1 protein to early endosomes via Endofin, as previously described by Seet et al., we used a 2xFYVE-Tom1 chimera construct to restore Tom1/clathrin interaction in Endofin-depleted cells (Seet and Hong, 2005). Of note, 2xFYVE-Tom1 chimera in Endofin-depleted cells lacks the ability to form a complex with Endofin binding partners once it is expressed, including HD-PTP. Our results showed that the complementation of Endofin-depleted HeLa cells with 2xFYVE-Tom1 chimera failed to restore EGFR lysosomal delivery (Figure S5G). Hence, although Endofin depletion reduced clathrin interaction with Tom1 and decreased clathrin recruitment to early endosomes, the delay in EGFR lysosomal delivery upon Endofin depletion is not directly linked to the loss of interaction between Endofin and Tom1 or to the role of Tom1 in receptor trafficking.

Endofin expression enhances HD-PTP colocalization with EGFR, Hrs and CHMP4B

HD-PTP directly interacts with ESCRT-0, -I, and -III proteins facilitating EGFR sorting toward MVBs and lysosomal degradation (Doyotte et al., 2008; Kharitidi et al., 2015). Endofin binds to the Bro1 domain of HD-PTP sharing the same binding site with STAM2 (ESCRT-0) and CHMP4B (ESCRT-III), however, Endofin binds HD-PTP with a higher affinity than STAM2 and CHMP4B (Gahloth et al., 2017b). In addition, STAM2 also binds to a motif in the proline rich region of HD-PTP, which serves as a second site for STAM2 interaction (Ali et al., 2013). To investigate whether Endofin could regulate HD-PTP complex formation with ESCRTs, endogenous HD-PTP was immunoprecipitated in Endofin-depleted cells and the co-IP efficiency of the ESCRT-0 protein Hrs was assessed. The indirect interaction of HD-PTP with Hrs was reduced by ~ 80% upon Endofin depletion (Figure 3A).

Since HD-PTP interaction with ESCRT-0 and -III on early endosomes is essential for the sorting of activated EGFR toward MVBs and lysosomes (Ali et al., 2013) (Doyotte et al., 2008) (Wenzel et al., 2018), we assessed in Endofin-depleted cells the colocalization of EGFR, red fluorescence protein-tagged Hrs (RFP-Hrs) and mCherry-tagged CHMP4B (mCherry-CHMP4B) with HD-PTP by pulse-chase experiments. EGFR colocalization with HD-PTP showed a significant decrease upon Endofin depletion (0.4 ± 0.03), after 5 min EGF stimulation and 10 min EGFR chase, compared to NT cells (0.54 ± 0.03) (Figure 3B). Consistent with the co-IP result, Hrs colocalization with HD-PTP, after 5 min EGF stimulation and 0 min EGFR chase, was significantly reduced upon Endofin depletion (0.44 ± 0.01) compared to NT cells (0.71 ± 0.03) (Figure 3C). Moreover, CHMP4B colocalization with HD-PTP also decreased upon Endofin depletion (0.44 ± 0.06) compared to NT cells (0.62 ± 0.05), after 5 min EGF stimulation and 20 min EGFR chase (Figure 3D). Therefore, this data suggests that EGFR, ESCRT-0 (Hrs), and ESCRT-III (CHMP4B) colocalizations and/or complex formation with HD-PTP are promoted by Endofin, which facilitates EGFR sorting toward MVBs and lysosomal degradation via ESCRT-dependent mechanisms.

Next, the colocalization of EGFR and RFP-Hrs with Endofin was also assessed in HD-PTP-depleted cells by pulse-chase experiments. We found that the colocalizations of EGFR and Hrs with Endofin are stabilized upon HD-PTP depletion after 5 min EGF stimulation and until 20 min EGFR chase. However, EGFR and Hrs showed dynamic colocalizations with Endofin in NT cells (Figures S6A and S6B). This infers that the dynamic colocalizations of EGFR and Hrs with Endofin are regulated by HD-PTP. This dynamic colocalization

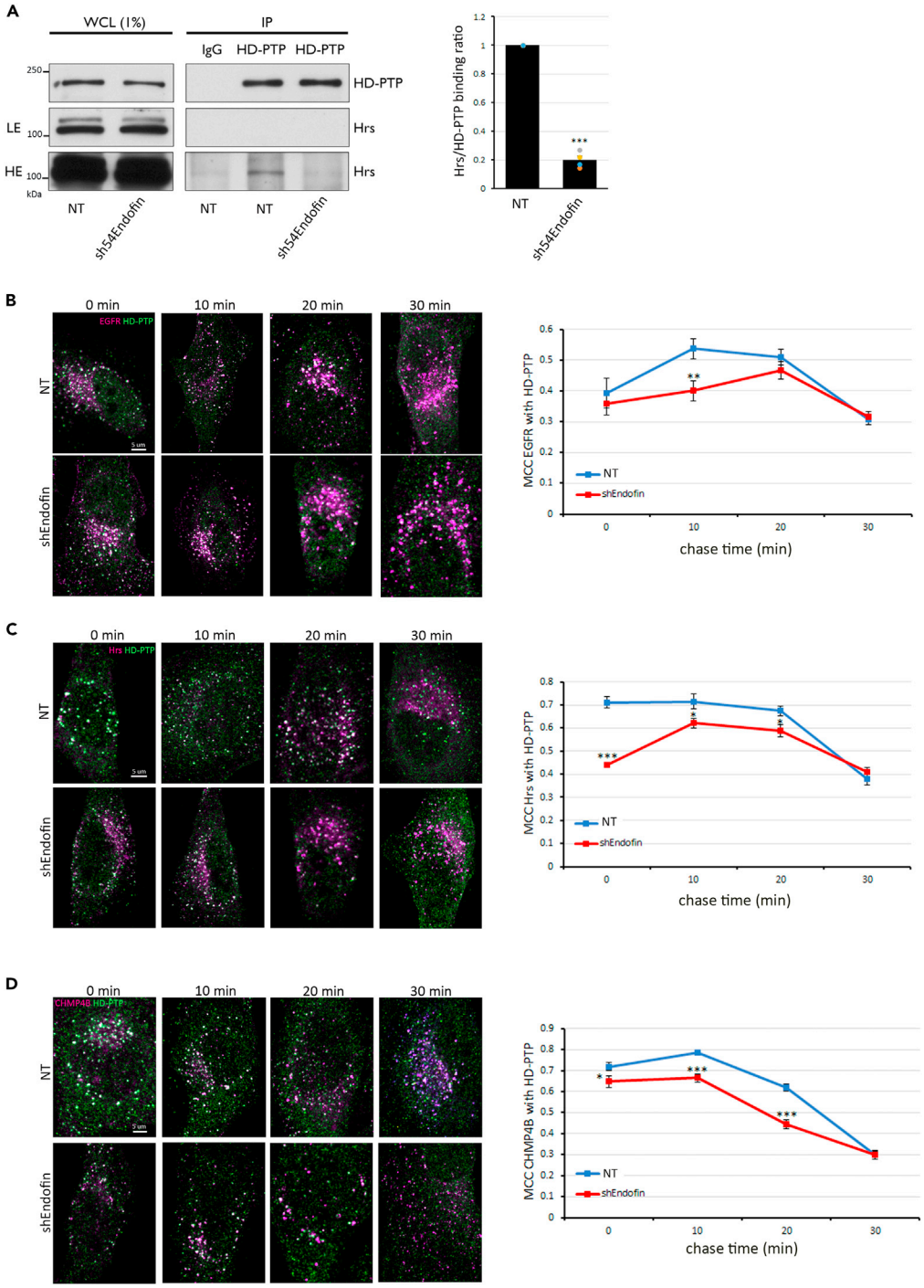

Figure 3. Endofin promotes HD-PTP colocalization with EGFR, Hrs and CHMP4B

(A) Co-IP performed on control and Endofin-depleted 293T cells upon EGF stimulation (50 ng/mL, 15 min, 37°C). Endogenous HD-PTP was immunoprecipitated and co-IP of Hrs was assessed by Western blotting. Whole cell lysate (WCL 1%) is loaded to reveal protein content.

(B–D)(B and C) Colocalization analysis of EGFR (B), Hrs (C) and CHMP4B (D) with HD-PTP in Endofin-depleted HeLa cells. Serum-starved cells were stimulated with EGF (50 ng/mL, 5 min, 37°C) then EGFR was chased for 0, 10, 20 and 30 min at 37°C. Mander's Colocalization Coefficient (MCC) was quantified using ImageJ software (n = 30). Representative immunofluorescence images are shown for each time point. Data are mean ± SEM of n ≥ 3 independent experiments. Unpaired student t-test: *p < 0.05, **p < 0.01, ***p < 0.001.

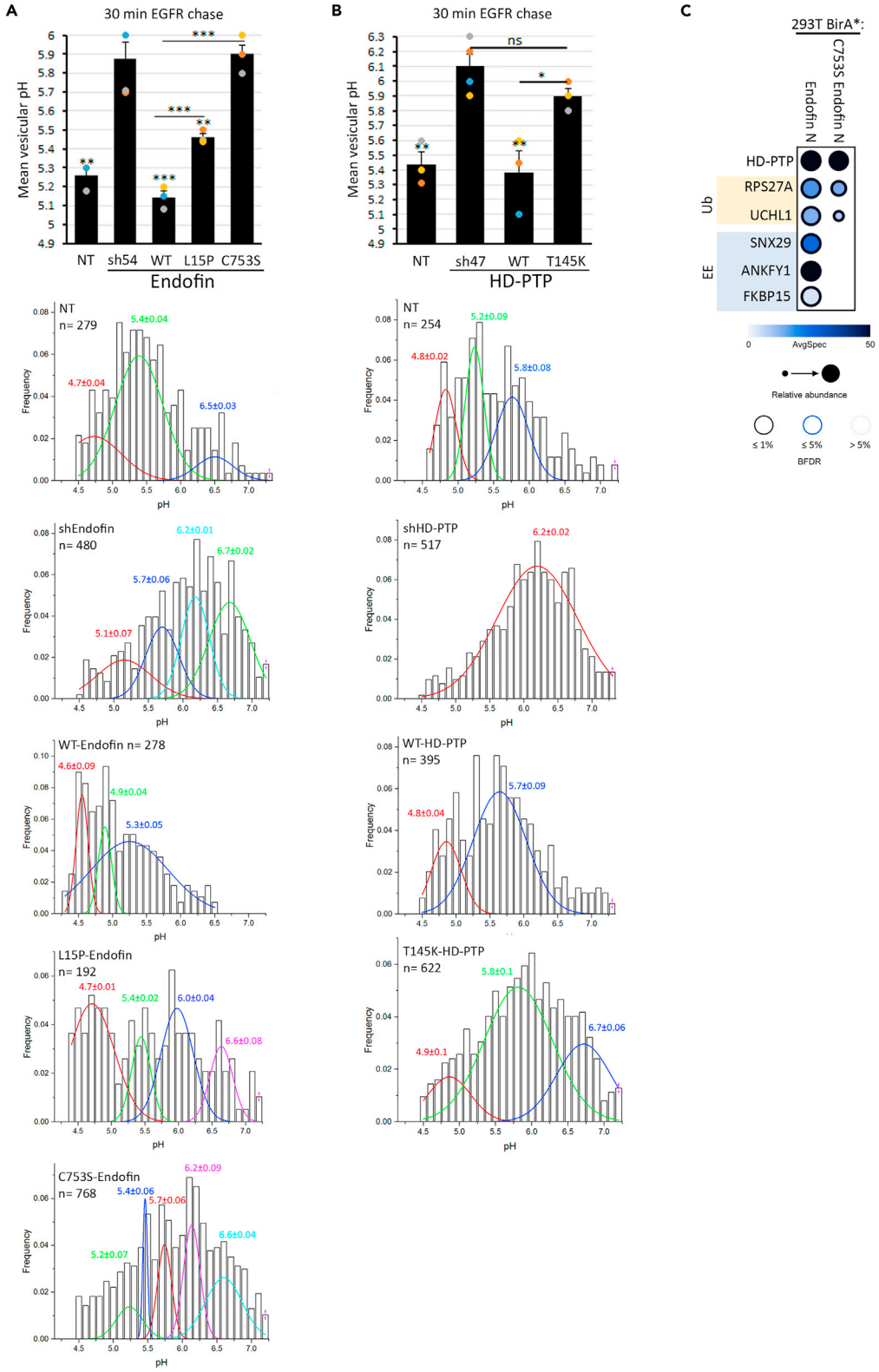

Figure 4. Endofin/HD-PTP interaction is permissive for an efficient lysosomal delivery of activated EGFR

(A and B) Mean vesicular pH of FITC-labeled EGFR-containing endocytic vesicles determined by FRIA, after 30 min of EGFR chase (50 ng/mL EGF, 37°C), in (A) Endofin-depleted HeLa cells transiently co-transfected with mCherry plasmid

Figure 4. *Continued*
and Flag-tagged WT-, L15P- or C753S-Endofin constructs, or (B) HD-PTP-depleted HeLa cells transiently co-transfected with mCherry plasmid, WT- or T145K-HD-PTP (disrupts HD-PTP interaction with Endofin) constructs. Single cell FRIA analysis was performed on cells expressing mCherry (vesicles: n > 190, microscopic fields: n > 10). Vesicular pH distribution of internalized EGFR after 30 min of EGFR chase is plotted. The mean vesicular pH of the distinct peaks and the number of vesicles in NT, shEndofin, WT-Endofin, L15P-Endofin, C753S-Endofin, shHD-PTP- and T145K-HD-PTP HeLa cells are indicated.
(C) Dot plot of BioID screen showing proteins related to ubiquitination (Ub) and early endosomes (EE) in close proximity to WT-Endofin and C753S-Endofin. Flag-tagged biotin ligase (BirA*) was fused to the N-terminus of WT-Endofin and C753S-Endofin and were used as baits. Constructs were transfected into Flp-In T-REx 293T cells. Fill shades in the dot plot indicate the average spectral counts (Avg Spec), the size of the dot represents its relative abundance across all preys and the outer circle color represents the BFDR value. Data are mean ± SEM of n ≥ 3 independent experiments. Unpaired student t-test: *p < 0.05, **p < 0.01, ***p < 0.001.

might reflect the egress of cargoes from early endosomes toward MVBs and lysosomes, which is indeed regulated by HD-PTP (Doyotte et al., 2008). On the other hand, the stabilized colocalizations of EGFR and Hrs with Endofin upon HD-PTP depletion might reflect the delay in cargo sorting from early endosomes toward MVBs and lysosomes.

Endofin/HD-PTP interaction is permissive for an efficient lysosomal delivery of activated EGFR

Endofin directly binds and recruits HD-PTP to early endosomes (Gahloth et al., 2017b). The double L202D/I206D-HD-PTP mutation, which abrogates CHMP4B and Endofin binding to HD-PTP, prevents L202D/I206D-HD-PTP recruitment to early endosomes even upon its co-expression with myc-Endofin (Gahloth et al., 2017b). Our data showed that EGFR and ESCRT-0 colocalizations with HD-PTP are stabilized by Endofin. To assess the functional aspect of Endofin/HD-PTP interaction in regulating cargo sorting toward MVBs and lysosomes, we generated shRNA resistant wild-type (WT) and mutant Endofin constructs.

Transient overexpression of the FYVE-domain C753S-Endofin mutant displayed an impaired localization to early endosomes, a finding we reciprocated here (Figure S6C) (Seet and Hong, 2001). To weaken Endofin's interaction with the Bro1 domain of HD-PTP (Gahloth et al., 2017a), we employed the L15P-Endofin mutant.

To investigate the effect of Endofin complementation on EGFR endo-lysosomal trafficking, pH_v of EGFR-containing vesicles was monitored by FRIA. Endofin-depleted HeLa cells were transiently transfected with WT- or mutated-Endofin (Figure S6D), and the mean pH_v was assessed after 30 min of EGF stimulation. WT-Endofin complementation restored EGFR lysosomal delivery (mean $pH_v \sim 5.1 \pm 0.03$) compared to mock transfected Endofin-depleted cells (mean $pH_v \sim 5.9 \pm 0.09$) and NT cells (mean $pH_v \sim 5.3 \pm 0.04$) (Figure 4A). L15P-Endofin complementation partially restored EGFR lysosomal delivery (mean $pH_v \sim 5.5 \pm 0.02$) compared to WT-Endofin (Figure 4A), in line with the partially disrupted biochemical interaction of L15P-Endofin with HD-PTP (Figure S6E). Conversely, C753S-Endofin complementation completely failed to rescue EGFR lysosomal delivery (mean $pH_v \sim 5.9 \pm 0.05$) (Figure 4A) by profoundly reducing Endofin recruitment to early endosomes.

Importantly, complementing HD-PTP-depleted HeLa cells with WT-HD-PTP (Figure S6D) restored EGFR lysosomal delivery (mean $pH_v \sim 5.4 \pm 0.15$) (Figure 4B). T145K-HD-PTP, which partially disrupted HD-PTP/Endofin interaction (Figure S6F) (Gahloth et al., 2017c), failed to rescue EGFR lysosomal delivery (mean $pH_v \sim 5.9 \pm 0.05$) compared to mock transfected HD-PTP-depleted (mean $pH_v \sim 6.1 \pm 0.08$) and NT (mean $pH_v \sim 5.4 \pm 0.09$) cells (Figure 4B).

To better understand the mechanism by which Endofin's FYVE domain influences HD-PTP's recruitment to early endosomes, we extended our BioID investigation to C753S-Endofin N-terminally BirA* tagged baits. Consistent with our findings, disruption of the FYVE domain did not reduce Endofin's interaction with HD-PTP but did disrupt its proximity interaction with ubiquitin and several early endosome components, providing an insight into a potential mechanism by which Endofin supports HD-PTP's recruitment to ubiquitinated cargoes on endocytic vesicles (Figure 4C). These results strongly suggest that both Endofin localization on early endosomes via its FYVE domain and its interaction with HD-PTP are necessary for an efficient endo-lysosomal transfer of activated EGFR.

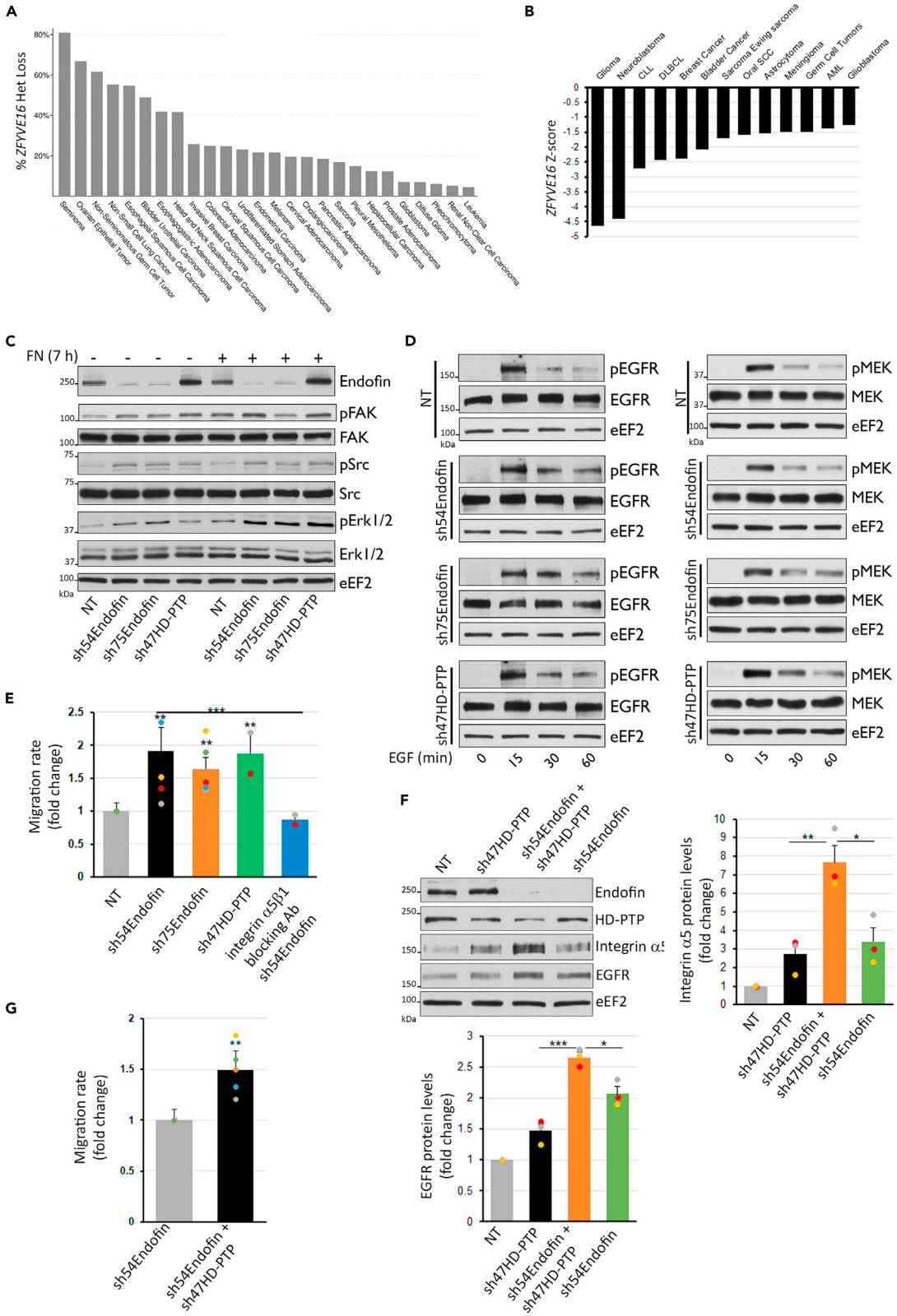
A
% ZFYVE16 Het Loss
80%
60%
40%
20%
Seminoma
Ovarian Epithelial Tumor
Non-Seminomatous Germ Cell Tumor
Non-Small Cell Lung Cancer
Bladder Urothelial Carcinoma
Esophagogastric Adenocarcinoma
Head and Neck Squamous Cell Carcinoma
Invasive Breast Carcinoma
Colorectal Adenocarcinoma
Cervical Squamous Cell Carcinoma
Undifferentiated Stomach Adenocarcinoma
Endometrial Carcinoma
Melanoma
Cervical Adenocarcinoma
Cholangiocarcinoma
Pancreatic Adenocarcinoma
Sarcoma
Pleural Mesothelioma
Hepatocellular Carcinoma
Prostate Adenocarcinoma
Glioblastoma
Diffuse Glioma
Pheochromocytoma
Renal Non-Clear Cell Carcinoma
Leukemia
B
ZFYVE16 Z-score
0
-0.5
-1
-1.5
-2
-2.5
-3
-3.5
-4
-4.5
-5
Glioma
Neuroblastoma
CLL
DLBCL
Breast Cancer
Bladder Cancer
Sarcoma Ewing sarcoma
Oral SCC
Astrocytoma
Meningioma
Germ Cell Tumors
AML
Glioblastoma
C
FN (7 h) - - - - + + + +
Endofin
pFAK
FAK
pSrc
Src
pErk1/2
Erk1/2
eEF2
kDa
NT
sh54Endofin
sh75Endofin
sh47HD-PTP
D
NT
pEGFR
EGFR
eEF2
pMEK
MEK
sh54Endofin
sh75Endofin
sh47HD-PTP
EGF (min) 0 15 30 60
E
Migration rate (fold change)
NT
sh54Endofin
sh75Endofin
sh47HD-PTP
integrin α5β1 blocking Ab sh54Endofin
F
NT
sh47HD-PTP
sh54Endofin + sh47HD-PTP
sh54Endofin
Endofin
HD-PTP
Integrin α5
EGFR
eEF2
Integrin α5 protein levels (fold change)
EGFR protein levels (fold change)
G
Migration rate (fold change)
sh54Endofin
sh54Endofin + sh47HD-PTP

Figure 5. Endofin depletion sustains integrin α5 and EGFR downstream signaling and increases cell migration

(A) Frequency of heterozygous loss of *ZFYVE16* (Endofin gene) in human patients with different types of cancers. Data extracted from cBioPortal database and plotted as the percentage of patients with *ZFYVE16* heterozygous loss.

(B) Z-score analysis of Endofin in human patients with different types of cancers. Endofin Z-score for each cancer type was extracted from PRECOG database and plotted.

(C) Western blots showing the phosphorylation levels of integrin α5 receptor downstream effectors: FAK, Src and Erk1/2 in Endofin- and HD-PTP-depleted HeLa cells compared to NT cells after fibronectin stimulation (10 μg/mL FN, 7 h, 37°C). eEF2 blots serve as a loading control.

(D) Endofin- and HD-PTP-depleted HeLa cells compared to NT cells were stimulated with EGF (5 ng/mL, 37°C) for 0-, 15-, 30- and 60-min. Western blots were performed to reveal the phosphorylation state of EGFR (left panel) and its downstream effector MEK (right panel). eEF2 blots serve as a loading control.

(E) Real time cell analysis (RTCA) measuring cell migration in Endofin- and HD-PTP-depleted HeLa cells compared to NT cells. Cell culture media supplemented with 10% FBS was used as a chemoattractant to trigger cell migration. Serum-free media (absence of chemoattractant) was used as a negative control. Integrin α5β1 blocking antibody (10 μg/mL) was used as a negative control to inhibit cell migration in Endofin-depleted cells.

(F) Endofin-depleted or control HeLa cells were transiently transfected with a non-targeting (NT) shRNA or with HD-PTP shRNA. Receptor levels were assessed by Western blotting and quantified by densitometric analysis using ImageJ software.

(G) Real time cell analysis was performed as in (E) to compare the migration rate of Endofin-depleted cells transiently transfected with either HD-PTP shRNA or NT control. Data are mean ± SEM of $n \geq 3$ independent experiments. Unpaired student t-test: *$p < 0.05$, **$p < 0.01$, ***$p < 0.001$.

Endofin depletion sustains integrin α5 and EGFR downstream signaling

We previously showed that the heterozygous loss of *PTPN23* is frequent in several types of human cancers (Manteghi et al., 2016). Using the cBioPortal database, we show here that the heterozygous loss of *ZFYVE16* (Endofin gene) is also frequent in several types of human cancers (Figure 5A). In addition, the PRECOG database, which measures associations between mRNA expression profiles and cancer prognosis by calculating a Z-score, revealed a negative Z-score of *ZFYVE16* mRNA in several types of human cancers (Figure 5B).

Cell surface receptors are competent of signaling from early endosomes or MVBs before the formation of ILVs (Mamińska et al., 2016; Rodahl et al., 2009; Wegner et al., 2011). Furthermore, HD-PTP depletion was shown to delay integrin α5 lysosomal delivery, thereby increasing its downstream signaling (Kharitidi et al., 2015). To investigate whether Endofin could also influence integrin α5 signaling, Endofin- and HD-PTP-depleted HeLa cells were stimulated with fibronectin (7 h) to assess levels of phosphorylated FAK, Src and Erk1/2 by Western blotting. In agreement with our previous study, HD-PTP depletion in serum-starved cells increased the levels of pFAK, pSrc, and pErk1/2 compared to NT cells, both at steady state and upon fibronectin stimulation (Figure 5C). Remarkably, the same effect was observed upon Endofin depletion (Figure 5C). This result clearly demonstrates that in addition to receptor stabilization, Endofin depletion further increased integrin α5 signaling.

Next, the effect of Endofin and HD-PTP depletion on EGFR activation and the kinetics of its downstream signaling were evaluated. Interestingly, Endofin and HD-PTP depletion had no significant impact on steady-state EGFR phosphorylation and the activation of its downstream kinase MEK (Figure 5D). However, EGFR and MEK activation were both sustained after 30 min of EGF stimulation upon Endofin and HD-PTP depletion. The levels of pEGFR also remained higher in these cells, even after 60 min of EGF stimulation (Figure 5D). Altogether, these results indicate that Endofin and HD-PTP do not only regulate EGFR and integrin α5 plasma membrane stability, but also control receptor activation and its downstream signaling.

Endofin depletion increases cell migration

Integrin α5β1's central role in cell migration and its ESCRT-dependent lysosomal desensitization are well established (Kharitidi et al., 2015; Lobert et al., 2010). The migration rate of Endofin-depleted HeLa cells was measured by real time cell analysis (RTCA) using fetal bovine serum as a chemoattractant. Endofin depletion revealed the same effect on cell migration rate as HD-PTP depletion with ~ 2-fold increase compared to NT cells. Migration of Endofin-depleted cells was suppressed by integrin α5β1 blocking antibody (Figure 5E). This shows that the increase in cell migration upon Endofin depletion is linked to the increase of PM and total integrin α5 levels (Figures 2C and S4B).

Since Endofin/HD-PTP interaction is permissive for an efficient lysosomal delivery of activated EGFR (Figures 4B and 4C), we next addressed whether simultaneous depletion of Endofin and HD-PTP could further impair receptor trafficking. Thus, we compared total EGFR and integrin α5 levels between NT and Endofin-depleted cells, transiently transfected either with a non-targeting shRNA or an shRNA targeting HD-PTP. We found that depleting Endofin or HD-PTP increased total EGFR levels by ~ 2-fold and ~1.5-fold,

respectively, whereas EGFR levels in double knock-down cells increased by ~2.7-fold in comparison to NT cells (Figure 5F). Interestingly, the impact was even more pronounced for integrin α5. Indeed, the individual depletion of Endofin or HD-PTP increased integrin α5 levels by ~ 3.4-fold and ~2.7-fold, respectively, whereas double knocked-down cells exhibited ~7.7-fold increase in comparison to NT cells (Figure 5F). To address the functional relevance of these findings, we also performed migration assays using fetal bovine serum as a chemoattractant. Results showed that the migration rate increased in double knock-down cells by ~ 1.5-fold in comparison to Endofin-depleted cells (Figure 5G). Altogether, these results indicate that the simultaneous depletion of Endofin and HD-PTP has an additive effect on total receptor levels, which in turn increase their migration rate in comparison to Endofin-depleted cells.

In certain types of human cancers, integrin α5 and EGFR are well-known drivers of tumorigenesis. Here, we show that Endofin depletion increased integrin α5 and EGFR signaling and cell migration, which are two hallmarks of cancer progression. Hence, loss of Endofin expression delays receptor lysosomal degradation and increases receptor signaling and cell migration, which could ultimately contribute to tumorigenesis and cancer progression.

DISCUSSION

Here, we unraveled the role of Endofin in promoting HD-PTP complex formation with ESCRT-0 on early endosomes to secure efficient ESCRT-dependent lysosomal degradation of internalized and ubiquitinated cell surface receptors and other transmembrane cargoes, a process which also desensitizes activated receptors (Wegner et al., 2011), controls cell migration (Kharitidi et al., 2015; Lobert et al., 2010; Lobert and Stenmark, 2012), and PM proteostasis (Apaja and Lukacs, 2014). Our findings can be summarized as follows: 1) Endofin forms complexes with ESCRT and HD-PTP proteins as well as EGFR on early endosomes. 2) The FYVE domain-dependent endosomal tether of Endofin and HD-PTP is required for the activated EGFR efficient lysosomal delivery, which is compromised by cytosolic relocation of Endofin or preventing its association with HD-PTP. 3) Endofin is also critical for poly-ubiquitinated but not multi-mono-ubiquitinated lysosomal delivery of model transmembrane cargoes which lack signaling capacity. 4) Endofin depletion, similar to HD-PTP haploinsufficiency, sustained EGF and integrin α5 receptor signaling and increased cell migration.

Segregation of internalized transmembrane cargoes into different microdomains on early endosomes is directed by specific sorting motifs toward the tubulovesicular recycling route, retrograde traffic to the Golgi complex, or toward MVB/lysosomal degradation (Norris et al., 2017). Upon ligand stimulation, EGFR undergoes both K63 poly-ubiquitination and multi-mono-ubiquitination (Huang et al., 2006), while integrin α5β1 is poly-ubiquitinated (Kharitidi et al., 2015; Lobert et al., 2010), serving as both internalization and endo-lysosomal sorting signals (Piper et al., 2014). Ubiquitinated cargoes are recognized cooperatively by multiple low-affinity ubiquitin-binding domains of ESCRT-0 and -I proteins, including Hrs, STAM2, UBAP1, and Tsg101, which are concentrated at the double-layer clathrin coat (Agromayor et al., 2012; Bache et al., 2003; Raiborg et al., 2002; Sundquist et al., 2004). In addition, Tom1 and HD-PTP, binding partners of Endofin, can recognize the poly- and mono-ubiquitinated moieties via their GAT + VHS- and V-domain, respectively, fostering cargo concentration on the limiting membrane of early endosomes (Akutsu et al., 2005; Pashkova et al., 2013; Wang et al., 2010).

While the lysosomal sorting of activated receptors and MVB biogenesis requires the dynamic interaction of HD-PTP with STAM2, Tsg101, UBAP1, and CHMP4B (Ali et al., 2013; Gahloth et al., 2016, 2017b; Ichioka et al., 2007), the functional significance of Endofin remained enigmatic in this process (Gahloth et al., 2017b). As Endofin complex formation with Tom1 recruits clathrin and binds both directly and via Tollip to ubiquitin on early endosomes (Katoh et al., 2004; Seet and Hong, 2005; Seet et al., 2004), we assumed that Endofin may participate in endosomal sorting of ubiquitinated cargoes. This possibility was also supported by the role of Endofin in TGFβ/BMP signaling (Chen et al., 2007a; Shi et al., 2007) and Endofin complex formation with ESCRT-I (UBAP1, TSG101, Vps37A, Vps28) (Figure S1B). The functionality of the Endofin interaction networks was revealed by Endofin ablation that stabilized the PM/endosomal pool of EGF and integrin α5 receptors (Figure 2), phenocopying the consequences of HD-PTP, Hrs or Tsg101 depletion (Ali et al., 2013; Bache et al., 2006; Doyotte et al., 2008; Kharitidi et al., 2015; Lu et al., 2003; Ma et al., 2015; Parkinson et al., 2015; Wenzel et al., 2018). Although EGFR internalization remained unaltered by Endofin depletion, it induced receptor accumulation in early endosomes and at the PM, presumably by fostering its recycling. Accelerated recycling of internalized integrin α5β1 was also observed upon HD-PTP depletion (Kharitidi et al., 2015).

Clathrin is known to be recruited to early endosomes via two different clathrin-binding proteins: Hrs and Tom1 (Raiborg et al., 2001; Seet and Hong, 2005). Dynamic assembly and disassembly of clathrin on early endosomes is essential for cargo and ESCRT-0 clustering into microdomains and subsequent ILV formation (Raiborg et al., 2001; Sachse et al., 2002; Wegner et al., 2011; Wenzel et al., 2018). A significant contribution of Endofin via Tom1 in the double-layer clathrin formation (Seet and Hong, 2005), however, could be excluded as the 2xFYVE-Tom1 chimera failed to rescue EGFR lysosomal delivery in Endofin-depleted cells. We favor the model that Endofin binding to HD-PTP (Gahloth et al., 2017b) may also facilitate EGFR transfer from ESCRT-0 (Hrs and STAM2) to ESCRT-I and -III, as a prelude toward MVB/lysosomal delivery (Ali et al., 2013). In support, the yeast HD-PTP homologue Bro1 also binds to clathrin (Pashkova et al., 2013), consistent with our observation that HD-PTP top hit interactor was clathrin by AP-MS (Figure S1B). Thus Endofin/HD-PTP interaction on early endosomes might be a key event for sorting EGFR toward lysosomal degradation, which was demonstrated by our complementation with Endofin and HD-PTP variants, where the deletion of Endofin FYVE-domain also suppressed the recruitment of HD-PTP to early endosomes. In line, expression of the L202D/I206D-HD-PTP variant, lacking both Endofin and CHMP4B bindings, prevented HD-PTP recruitment to early endosomes even upon its co-expression with myc-Endofin (Gahloth et al., 2017c).

Considering that ligand-stimulated poly-ubiquitination serves as a critical recognition signal for integrin α5 and EGFR engagement with the ESCRT machinery (Eden et al., 2012; Kharitidi et al., 2015; Lobert et al., 2010), we propose that dynamic Endofin-ESCRT association is a prerequisite for routing a panel of ubiquitinated cargo molecules from early endosomes toward MVB/lysosomes independently of the receptors downstream signaling. This inference is supported by Endofin-dependent lysosomal delivery of the poly-ubiquitinated (CD4TI-Ub) model cargo, but not tetrameric mono-ubiquitinated (CD4TCC-UbAllRΔG) (Figures 2F and 2G), mono-ubiquitinated (CD4TI-UbRΔG) or the CD4TI model cargo, which lacks a ubiquitin acceptor site (Barriere et al., 2006, 2007). These results also raise the possibility that the ESCRT machinery-driven ubiquitin-chain selectivity may be influenced by the ESCRT complex composition, including Endofin. This corollary is in line with Endofin-dependent regulation of TGFβ/BMP receptor that undergoes ligand-induced K63 poly-ubiquitination (Chen et al., 2007a; Iyengar, 2017). Thus, downregulation of Endofin in cancer cells may differentially alter the cell surface receptor proteome and signaling pending their ubiquitin-chain modification, which in turn could perturb downstream signaling cascades and transcriptional pathways.

The endosomal signaling of internalized receptors is terminated upon receptor budding into ILVs during MVB biogenesis (Platta and Stenmark, 2011; Wegner et al., 2011). Integrin α5β1 and EGFR uncontrolled signaling plays a major role in cell migration and cancer metastasis (Mierke et al., 2011; Yamaguchi et al., 2005). Sustained signaling of both integrin α5 and EGFR upon Endofin depletion, could be linked to the accumulation of EGFR at early endosomes and their delayed MVB/lysosome sorting (Figure 2D). Moreover, the blockage of integrin α5β1 activation and coupled ubiquitination (Kharitidi et al., 2015) demonstrate that elevated PM level of integrin α5 is, at least partly, responsible for accelerated cell migration (Figure 5E). Augmented PM expression and downstream signaling of integrin α5 were also associated with accelerated cell migration upon HD-PTP depletion (Kharitidi et al., 2015), consistent with the importance of Endofin/HD-PTP interaction in regulating ESCRT-dependent receptor trafficking, receptor signaling and cell migration.

It has been shown that Hrs and STAM2, similar to Endofin, undergo phosphorylation upon EGF stimulation (Chen et al., 2007b; Pandey et al., 2000; Row et al., 2005). The sorting of internalized receptors triggers Hrs phosphorylation, promoting its dislocation from early endosomes (Urbé et al., 2000). Based on published data and our findings, we propose the following working model for Endofin role in the endo-lysosomal trafficking of ligand-activated and ubiquitinated cell surface receptors. Endofin, via its FYVE-dependent endosomal localization and binding to HD-PTP, facilitates HD-PTP recognition of ubiquitinated endosomal cargo in complex with STAM2 and Hrs (ESCRT-0), clathrin recruitment, and cargo clustering at endosomal microdomains. Subsequent dissociation of Endofin from HD-PTP (and STAM2) enables CHIMP4B/HD-PTP association by a presently poorly understood mechanism. We speculate that this process may be facilitated by the post-translational modification(s) favoring the dissociation of Endofin/HD-PTP, similar to that observed for the phosphorylation-induced Hrs dissociation from endosomes (Urbé et al., 2000). Furthermore, cargo loading and assembly of ESCRT-0/-I with HD-PTP may induce allosteric Endofin dissociation from the complex. Testing and refining this model will be accomplished by monitoring the kinetics of

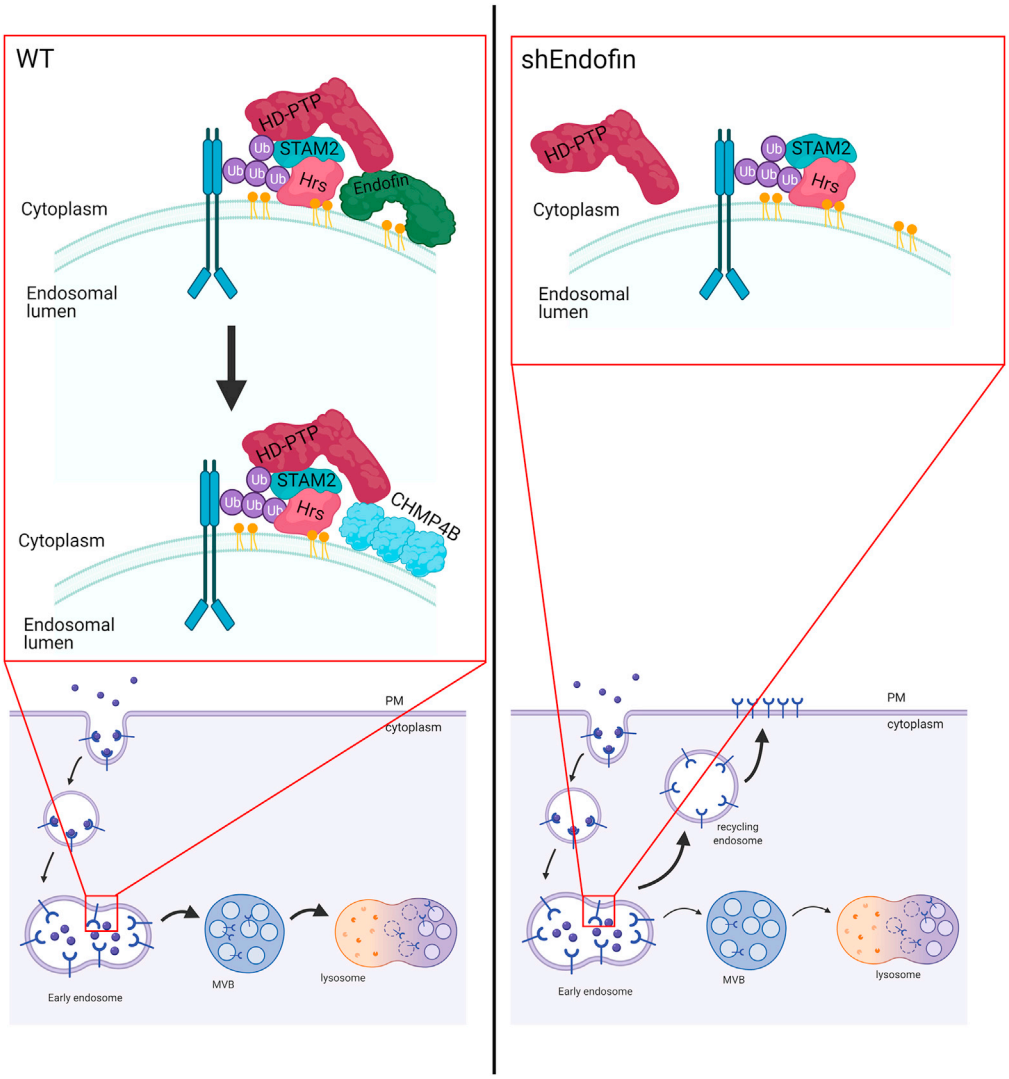

Figure 6. Schematic model of Endofin's role in receptor trafficking

After internalized receptors are targeted toward early endosomes in wild-type cells (WT), Endofin recruits HD-PTP to early endosomes via its FYVE-domain and their direct interaction. Endofin promotes HD-PTP interaction with ESCRT-0 on early endosomes, through STAM2 binding to the proline rich region of HD-PTP. Next, Endofin may undergo allosteric conformational modifications (probably by post-translational modifications), which weakens Endofin/HD-PTP association and facilitates HD-PTP/CHMP4B interaction. Eventually, this leads to an efficient ESCRT-dependent sorting of EGFR toward MVBs and lysosomal degradation. On the other hand, in Endofin-depleted cells (shEndofin), HD-PTP interaction with ESCRT-0 decreases, which favors receptor recycling back to the plasma membrane and delays ESCRT-dependent EGFR sorting toward MVBs and lysosomal degradation.

recruitment of fluorescent-tagged HD-PTP in relation to other ESCRTs in the presence of Endofin variants during cargo sorting by live-cell imaging and related to that described for concerted ESCRT and clathrin recruitment waves to early endosomes by Wenzel et al. (Wenzel et al., 2018). Furthermore, SARA protein, Endofin's homologue, also directly binds to HD-PTP and its recruitment to early endosomes (Gahloth et al., 2017b) might serve as a compensatory mechanism in an Endofin-depleted context. In summary, we propose that Endofin is required for HD-PTP mediated cargo transfer from ESCRT-0/-I to ESCRT-III on early endosomes, a critical step in lysosomal delivery of poly-ubiquitinated cargoes (Figure 6).

Disruption of Endofin/HD-PTP interaction (e.g., by Endofin mutants or *PTPN23* haploinsufficiency) leads to sustained EGF and integrin α5 receptor signaling (Figure 5) (Kharitidi et al., 2015; Manteghi et al., 2016),

including downstream transcriptional activation known to promote tumorigenesis and cancer progression (Hou et al., 2020; Sigismund et al., 2018). The heterozygous loss of *ZFYVE16* and downregulation of Endofin transcript in several types of human cancers (Figure 5) suggests that Endofin may exert a tumor suppressor activity, which requires further investigations.

Limitations of the study

In this study, we have characterized the role of Endofin in targeting integrin α5 and EGFR toward lysosomal degradation, thus regulating receptor signaling and cell migration. We have also shown that Endofin is required for HD-PTP association with ESCRT-0/-III for an efficient EGFR lysosomal delivery. However, the exact mechanism of Endofin association/dissociation with/from HD-PTP, ESCRTs and clathrin complex on early endosomes is still unknown. This will be an interesting direction for future research requiring advanced imaging techniques and protein structural analysis.

Furthermore, it is not fully known whether Endofin regulates the endo/lysosomal delivery of all cell surface receptors undergoing poly-ubiquitination upon activation. Further investigation would be required to address the effect of Endofin depletion on the global cell surface proteome, which might further influence downstream transcriptional pathways.

STAR★METHODS

Detailed methods are provided in the online version of this paper and include the following:

- KEY RESOURCES TABLE
- RESOURCE AVAILABILITY
  - Lead contact
  - Materials availability
  - Data and code availability
- EXPERIMENTAL MODEL AND SUBJECT DETAILS
  - Cell lines
- METHODS DETAILS
  - Constructs, reagents and cell culture
  - AP-MS cloning, stable cell line generation and sample collection
  - BioID cloning, stable cell line generation and sample collection
  - AP-MS and BioID sample processing and mass spectrometry analysis
  - Data-dependent and independent acquisition data searches
  - Proteomics data deposition
  - STRING analysis
  - Immunoprecipitation
  - Size-exclusion chromatography fractionation
  - Isopycnic sucrose gradient cellular fractionation
  - Cycloheximide chase
  - Cell surface measurements using cs-ELISA
  - Pulse chase experiments and immunofluorescence
  - Complementation experiments and vesicular cargo tracking using FRIA
  - HeLa cell migration assay
  - Signaling experiment
- QUANTIFICATION AND STATISTICAL ANALYSIS

SUPPLEMENTAL INFORMATION

Supplemental information can be found online at https://doi.org/10.1016/j.isci.2021.103274.

ACKNOWLEDGMENTS

We would like to thank Dr. Paola Blanchette for her help and advice. J.M.K holds Fonds de Recherche Sante (FRQS), Canada doctoral award. G.D holds Fonds de Recherche Sante (FRQS) post-doctoral award. This work was supported by the Canadian Institutes for Health Research (CIHR), Canada grant 245969 and the Canadian Cancer Society Research Institute (CCSRI), Canada grant 245095. Figure 6 was created using BioRender.com.

AUTHOR CONTRIBUTIONS

J.M.K., G.D., G.L.L. and A.P. carried out the study conceptualization and experimental design. J.M.K., G.D., C.E.M. performed experiments and analysis. H.J., D.K., P.M.A., A.R. and N.S.D. performed experiments. J.M.K., G.D., A.C.G., G.L.L., and A.P. wrote and edited the manuscript.

DECLARATION OF INTERESTS

The authors declare no competing financial interests.

Received: July 8, 2021
Revised: August 18, 2021
Accepted: October 12, 2021
Published: November 19, 2021

REFERENCES

Agromayor, M., Soler, N., Caballe, A., Kueck, T., Freund, S.M., Allen, M.D., Bycroft, M., Perisic, O., Ye, Y., and Mcdonald, B. (2012). The UBAP1 subunit of ESCRT-I interacts with ubiquitin via a SOUBA domain. Structure *20*, 414–428.

Akutsu, M., Kawasaki, M., Katoh, Y., Shiba, T., Yamaguchi, Y., Kato, R., Kato, K., Nakayama, K., and Wakatsuki, S. (2005). Structural basis for recognition of ubiquitinated cargo by Tom1-GAT domain. FEBS Lett. *579*, 5385–5391.

Ali, N., Zhang, L., Taylor, S., Mironov, A., Urbé, S., and Woodman, P. (2013). Recruitment of UBPY and ESCRT exchange drive HD-PTP-dependent sorting of EGFR to the MVB. Curr. Biol. *23*, 453–461.

Alwan, H.A., Van Zoelen, E.J., and Van Leeuwen, J.E. (2003). Ligand-induced lysosomal epidermal growth factor receptor (EGFR) degradation is preceded by proteasome-dependent EGFR de-ubiquitination. J. Biol. Chem. *278*, 35781–35790.

Apaja, P.M., and Lukacs, G.L. (2014). Protein homeostasis at the plasma membrane. Physiology *29*, 265–277.

Apaja, P.M., Xu, H., and Lukacs, G.L. (2010). Quality control for unfolded proteins at the plasma membrane. J. Cell Biol. *191*, 553–570.

Bache, K.G., Raiborg, C., Mehlum, A., and Stenmark, H. (2003). STAM and Hrs are subunits of a multivalent ubiquitin-binding complex on early endosomes. J. Biol. Chem. *278*, 12513–12521.

Bache, K.G., Stuffers, S., Malerød, L., Slagsvold, T., Raiborg, C., Lechardeur, D., Wälchli, S., Lukacs, G.L., Brech, A., and Stenmark, H. (2006). The ESCRT-III subunit hVps24 is required for degradation but not silencing of the epidermal growth factor receptor. Mol. Biol. Cel. *17*, 2513–2523.

Barriere, H., and Lukacs, G.L. (2008). Analysis of endocytic trafficking by single-cell fluorescence ratio imaging. Curr.Protoc.Cel.Biol. *40*, 15.13.1–15.13.21.

Barriere, H., Nemes, C., Du, K., and Lukacs, G.L. (2007). Plasticity of polyubiquitin recognition as lysosomal targeting signals by the endosomal sorting machinery. Mol. Biol. Cel. *18*, 3952–3965.

Barriere, H., Nemes, C., Lechardeur, D., Khan-Mohammad, M., Fruh, K., and Lukacs, G.L. (2006). Molecular basis of oligoubiquitin-dependent internalization of membrane proteins in Mammalian cells. Traffic *7*, 282–297.

Belle, L., Ali, N., Lonic, A., Li, X., Paltridge, J.L., Roslan, S., Herrmann, D., Conway, J.R., Gehling, F.K., Bert, A.G., et al. (2015). The tyrosine phosphatase PTPN14 (Pez) inhibits metastasis by altering protein trafficking. Sci.Signal *8*, ra18.

Budzinska, M.I., Villarroel-Campos, D., Golding, M., Weston, A., Collinson, L., Snijders, A.P., and Schiavo, G. (2020). PTPN23 binds the dynein adaptor BICD1 and is required for endocytic sorting of neurotrophin receptors. J.Cell Sci *133*.

Chen, Y.-G., Wang, Z., Ma, J., Zhang, L., and Lu, Z. (2007a). Endofin, a FYVE domain protein, interacts with Smad4 and facilitates transforming growth factor-β signaling. J. Biol. Chem. *282*, 9688–9695.

Chen, Y., Low, T.Y., Choong, L.Y., Ray, R.S., Tan, Y.L., Toy, W., Lin, Q., Ang, B.K., Wong, C.H., and Lim, S. (2007b). Phosphoproteomics identified Endofin, DCBLD2, and KIAA0582 as novel tyrosine phosphorylation targets of EGF signaling and Iressa in human cancer cells. Proteomics *7*, 2384–2397.

Christ, L., Raiborg, C., Wenzel, E.M., Campsteijn, C., and Stenmark, H. (2017). Cellular functions and molecular mechanisms of the ESCRT membrane-scission machinery. Trends Biochemical Sciences *42*, 42–56.

Desrochers, G., Kazan, J.M., and Pause, A. (2019). Structure and functions of His domain protein tyrosine phosphatase in receptor trafficking and cancer (1). Biochem.Cell Biol *97*, 68–72.

Doyotte, A., Mironov, A., Mckenzie, E., and Woodman, P. (2008). The Bro1-related protein HD-PTP/PTPN23 is required for endosomal cargo sorting and multivesicular body morphogenesis. Proc. Natl. Acad. Sci. *105*, 6308–6313.

Eden, E.R., Huang, F., Sorkin, A., and Futter, C.E. (2012). The role of EGF receptor ubiquitination in regulating its intracellular traffic. Traffic *13*, 329–337.

Elias, J.E., and Gygi, S.P. (2007). Target-decoy search strategy for increased confidence in large-scale protein identifications by mass spectrometry. Nat. Methods *4*, 207–214.

Gahloth, D., Heaven, G., Jowitt, T.A., Mould, A.P., Bella, J., Baldock, C., Woodman, P., and Tabernero, L. (2017a). The open architecture of HD-PTP phosphatase provides new insights into the mechanism of regulation of ESCRT function. Scientific Rep. *7*, 9151.

Gahloth, D., Levy, C., Heaven, G., Stefani, F., Wunderley, L., Mould, P., Cliff, M.J., Bella, J., Fielding, A.J., and Woodman, P. (2016). Structural basis for selective interaction between the ESCRT regulator HD-PTP and UBAP1. Structure *24*, 2115–2126.

Gahloth, D., Levy, C., Walker, L., Wunderley, L., Mould, A.P., Taylor, S., Woodman, P., and Tabernero, L. (2017b). Structural basis for specific interaction of TGFβ signaling regulators SARA/Endofin with HD-PTP. Structure *25*, 1011–1024.e4.

Gahloth, D., Levy, C., Walker, L., Wunderley, L., Mould, A.P., Taylor, S., Woodman, P., and Tabernero, L. (2017c). Structural basis for specific interaction of TGFβ signaling regulators SARA/Endofin with HD-PTP. Structure *25*, 1011–1024.e4.

Gingras, M.-C., Zhang, Y.L., Kharitidi, D., Barr, A.J., Knapp, S., Tremblay, M.L., and Pause, A. (2009). HD-PTP is a catalytically inactive tyrosine phosphatase due to a conserved divergence in its phosphatase domain. PLoS ONE *4*, e5105.

Goh, J.B., Wallace, D.F., Hong, W., and Subramaniam, V.N. (2015). Endofin, a novel BMP-SMAD regulator of the iron-regulatory hormone, hepcidin. Scientific Rep. *5*.

Hesketh, G.G., Papazotos, F., Pawling, J., Rajendran, D., Knight, J.D., Martinez, S., Taipale, M., Schramek, D., Dennis, J.W., and Gingras, A.-C. (2020). The GATOR–Rag GTPase pathway inhibits mTORC1 activation by lysosome-derived amino acids. Science *370*, 351–356.

Hou, J., Du Yan, Y.L., Huang, P., and Cui, H. (2020). The roles of integrin α5β1 in human cancer. OncoTargets Ther. *13*, 13329.

Huang, F., Kirkpatrick, D., Jiang, X., Gygi, S., and Sorkin, A. (2006). Differential regulation of EGF receptor internalization and degradation by multiubiquitination within the kinase domain. Mol. Cel. *21*, 737–748.

Ichioka, F., Takaya, E., Suzuki, H., Kajigaya, S., Buchman, V.L., Shibata, H., and Maki, M. (2007). HD-PTP and Alix share some membrane-traffic related proteins that interact with their Bro1 domains or proline-rich regions. Arch. Biochem. Biophys. *457*, 142–149.

Iyengar, P.V. (2017). Regulation of ubiquitin enzymes in the TGF-β pathway. Int. J. Mol. Sci. *18*, 877.

Katoh, Y., Shiba, Y., Mitsuhashi, H., Yanagida, Y., Takatsu, H., and Nakayama, K. (2004). Tollip and Tom1 form a complex and recruit ubiquitin-conjugated proteins onto early endosomes. J. Biol. Chem. *279*, 24435–24443.

Kazan, J.M., Lukacs, G.L., Apaja, P.M., and Pause, A. (2019). Single Cell Fluorescence Ratio Image Analysis for Studying Escrt Function in Receptor Trafficking. The ESCRT Complexes (Springer).

Kharitidi, D., Apaja, P.M., Manteghi, S., Suzuki, K., Malitskaya, E., Roldan, A., Gingras, M.-C., Takagi, J., Lukacs, G.L., and Pause, A. (2015). Interplay of endosomal pH and ligand occupancy in integrin α5β1 ubiquitination, endocytic sorting, and cell migration. Cell Rep. *13*, 599–609.

Kim, S., Mischerikow, N., Bandeira, N., Navarro, J.D., Wich, L., Mohammed, S., Heck, A.J., and Pevzner, P.A. (2010). The generating function of CID, ETD, and CID/ETD pairs of tandem mass spectra: applications to database search. Mol. Cell Proteomics *9*, 2840–2852.

Knight, J.D., Choi, H., Gupta, G.D., Pelletier, L., Raught, B., Nesvizhskii, A.I., and Gingras, A.-C. (2017). ProHits-viz: a suite of web tools for visualizing interaction proteomics data. Nat. Methods *14*, 645–646.

Lahaie, S., Morales, D., Bagci, H., Hamoud, N., Castonguay, C.E., Kazan, J.M., Desrochers, G., Klar, A., Gingras, A.C., Pause, A., et al. (2019). The endosomal sorting adaptor HD-PTP is required for ephrin-B:EphB signalling in cellular collapse and spinal motor axon guidance. Sci. Rep. *9*, 11945.

Lambert, J.-P., Tucholska, M., Go, C., Knight, J.D., and Gingras, A.-C. (2015). Proximity biotinylation and affinity purification are complementary approaches for the interactome mapping of chromatin-associated protein complexes. J. Proteomics *118*, 81–94.

Lee, J., Oh, K.-J., Lee, D., Kim, B.Y., Choi, J.S., Ku, B., and Kim, S.J. (2016). Structural study of the HD-PTP Bro1 domain in a complex with the core region of STAM2, a subunit of ESCRT-0. PloS one *11*, e0149113.

Liu, G., Knight, J.D., Zhang, J.P., Tsou, C.-C., Wang, J., Lambert, J.-P., Larsen, B., Tyers, M., Raught, B., and Bandeira, N. (2016). Data independent acquisition analysis in ProHits 4.0. J. Proteomics *149*, 64–68.

Lobert, V.H., Brech, A., Pedersen, N.M., Wesche, J., Oppelt, A., Malerød, L., and Stenmark, H. (2010). Ubiquitination of α5β1 integrin controls fibroblast migration through lysosomal degradation of fibronectin-integrin complexes. DevelopmentalCel. *19*, 148–159.

Lobert, V.H., and Stenmark, H. (2012). The ESCRT machinery mediates polarization of fibroblasts through regulation of myosin light chain. J. Cel. Sci. *125*, 29–36.

Lu, Q., Hope, L.W., Brasch, M., Reinhard, C., and Cohen, S.N. (2003). TSG101 interaction with HRS mediates endosomal trafficking and receptor down-regulation. Proc. Natl. Acad. Sci. *100*, 7626–7631.

Ma, H., Wardega, P., Mazaud, D., Klosowska-Wardega, A., Jurek, A., Engstrom, U., Lennartsson, J., and Heldin, C.H. (2015). Histidine-domain-containing protein tyrosine phosphatase regulates platelet-derived growth factor receptor intracellular sorting and degradation. Cell Signal *27*, 2209–2219.

Mamińska, A., Bartosik, A., Banach-Orłowska, M., Pilecka, I., Jastrzębski, K., Zdżalik-Bielecka, D., Castanon, I., Poulain, M., Neyen, C., and Wolińska-Nizioł, L. (2016). ESCRT proteins restrict constitutive NF-κB signaling by trafficking cytokine receptors. Sci. Signal. *9*, ra8.

Manteghi, S., Gingras, M.-C., Kharitidi, D., Galarneau, L., Marques, M., Yan, M., Cencic, R., Robert, F., Paquet, M., and Witcher, M. (2016). Haploinsufficiency of the ESCRT component HD-PTP predisposes to cancer. Cell Rep. *15*, 1893–1900.

Mierke, C.T., Frey, B., Fellner, M., Herrmann, M., and Fabry, B. (2011). Integrin α5β1 facilitates cancer cell invasion through enhanced contractile forces. J. Cel. Sci. *124*, 369–383.

Miller, D.S.J., Bloxham, R.D., Jiang, M., Gori, I., Saunders, R.E., Das, D., Chakravarty, P., Howell, M., and Hill, C.S. (2018). The dynamics of TGF-beta signaling are dictated by receptor trafficking via the ESCRT machinery. Cell Rep *25*, 1841–1855.e5.

Norris, A., Tammineni, P., Wang, S., Gerdes, J., Murr, A., Kwan, K.Y., Cai, Q., and Grant, B.D. (2017). SNX-1 and RME-8 oppose the assembly of HGRS-1/ESCRT-0 degradative microdomains on endosomes. Proc. Natl. Acad. Sci. *114*, E307–E316.

Okiyoneda, T., Barrière, H., Bagdány, M., Rabeh, W.M., Du, K., Höhfeld, J., Young, J.C., and Lukacs, G.L. (2010). Peripheral protein quality control removes unfolded CFTR from the plasma membrane. Science *329*, 805–810.

Pandey, A., Fernandez, M.M., Steen, H., Blagoev, B., Nielsen, M.M., Roche, S., Mann, M., and Lodish, H.F. (2000). Identification of a novel immunoreceptor tyrosine-based activation motif-containing molecule, STAM2, by mass spectrometry and its involvement in growth factor and cytokine receptor signaling pathways. J. Biol. Chem. *275*, 38633–38639.

Parkinson, M.D., Piper, S.C., Bright, N.A., Evans, J.L., Boname, J.M., Bowers, K., Lehner, P.J., and LUZIO, J.P. (2015). A non-canonical ESCRT pathway, including histidine domain phosphotyrosine phosphatase (HD-PTP), is used for down-regulation of virally ubiquitinated MHC class I. Biochem. J. *471*, 79–88.

Pashkova, N., Gakhar, L., Winistorfer, S.C., Sunshine, A.B., Rich, M., Dunham, M.J., Yu, L., and Piper, R.C. (2013). The yeast Alix homolog Bro1 functions as a ubiquitin receptor for protein sorting into multivesicular endosomes. DevelopmentalCel. *25*, 520–533.

Piper, R.C., Dikic, I., and Lukacs, G.L. (2014). Ubiquitin-dependent sorting in endocytosis. Cold Spring Harbor Perspect.Biol. *6*, a016808.

Platta, H.W., and Stenmark, H. (2011). Endocytosis and signaling. Curr.Opin.Cel. Biol. *23*, 393–403.

Raiborg, C., Bache, K.G., Gillooly, D.J., Madshus, I.H., Stang, E., and Stenmark, H. (2002). Hrs sorts ubiquitinated proteins into clathrin-coated microdomains of early endosomes. Nat. Cel. Biol. *4*, 394–398.

Raiborg, C., Bache, K.G., Mehlum, A., Stang, E., and Stenmark, H. (2001). Hrs recruits clathrin to early endosomes. EMBO J. *20*, 5008–5021.

Raiborg, C., Wesche, J., Malerod, L., and Stenmark, H. (2006). Flat clathrin coats on endosomes mediate degradative protein sorting by scaffolding Hrs in dynamic microdomains. J.Cell Sci *119*, 2414–2424.

Rodahl, L.M., Stuffers, S., Lobert, V.H., and Stenmark, H. (2009). The role of ESCRT proteins in attenuation of cell signalling. Biochem. Soc. Trans. *37*, 137–142.

Rosenberger, G., Koh, C.C., Guo, T., Röst, H.L., Kouvonen, P., Collins, B.C., Heusel, M., Liu, Y., Caron, E., and Vichalkovski, A. (2014). A repository of assays to quantify 10,000 human proteins by SWATH-MS. Scientific data *1*, 1–15.

Row, P.E., Clague, M.J., and Urbé, S. (2005). Growth factors induce differential phosphorylation profiles of the Hrs–STAM complex: a common node in signalling networks with signal-specific properties. Biochem. J. *389*, 629–636.

Sachse, M., Urbé, S., Oorschot, V., Strous, G.J., and Klumperman, J. (2002). Bilayered clathrin coats on endosomal vacuoles are involved in protein sorting toward lysosomes. Mol. Biol. Cel. *13*, 1313–1328.

Seet, L.F., and Hong, W. (2001). Endofin, an endosomal FYVE domain protein. J. Biol. Chem. *276*, 42445–42454.

Seet, L.-F., and Hong, W. (2005). Endofin recruits clathrin to early endosomes via TOM1. J. Cel. Sci. *118*, 575–587.

Seet, L.-F., Liu, N., Hanson, B.J., and Hong, W. (2004). Endofin recruits TOM1 to endosomes. J. Biol. Chem. *279*, 4670–4679.

Shi, W., Chang, C., Nie, S., Xie, S., Wan, M., and Cao, X. (2007). Endofin acts as a Smad anchor for receptor activation in BMP signaling. J. Cel. Sci. *120*, 1216–1224.

Sigismund, S., Avanzato, D., and Lanzetti, L. (2018). Emerging functions of the EGFR in cancer. Mol. Oncol. *12*, 3–20.

Sorkin, A., and von Zastrow, M. (2009). Endocytosis and signalling: intertwining molecular networks. Nat. Rev. Mol. Cel. Biol. *10*, 609–622.

St-Denis, N., Gupta, G.D., Lin, Z.Y., Gonzalez-Badillo, B., Veri, A.O., Knight, J.D., Rajendran, D., Couzens, A.L., Currie, K.W., and Tkach, J.M. (2016). Phenotypic and interaction profiling of the

human phosphatases identifies diverse mitotic regulators. Cell Rep. *17*, 2488–2501.

Stefani, F., Zhang, L., Taylor, S., Donovan, J., Rollinson, S., Doyotte, A., Brownhill, K., Bennion, J., Pickering-Brown, S., and Woodman, P. (2011). UBAP1 is a component of an endosome-specific ESCRT-I complex that is essential for MVB sorting. Curr. Biol. *21*, 1245–1250.

Sundquist, W.I., Schubert, H.L., Kelly, B.N., Hill, G.C., Holton, J.M., and Hill, C.P. (2004). Ubiquitin recognition by the human TSG101 protein. Mol. Cel. *13*, 783–789.

Szklarczyk, D., Gable, A.L., Lyon, D., Junge, A., Wyder, S., Huerta-Cepas, J., Simonovic, M., Doncheva, N.T., MORRIS, J.H., and BORK, P. (2019). STRING v11: protein–protein association networks with increased coverage, supporting functional discovery in genome-wide experimental datasets. Nucleic Acids Res. *47*, D607–D613.

Szymanska, E., Budick-Harmelin, N., and Miaczynska, M. (2018). Endosomal "sort" of signaling control: the role of ESCRT machinery in regulation of receptor-mediated signaling pathways. Semin.Cell Dev Biol *74*, 11–20.

Teo, G., Liu, G., Zhang, J., Nesvizhskii, A.I., Gingras, A.-C., and Choi, H. (2014). SAINTexpress: improvements and additional features in Significance Analysis of INTeractome software. J. Proteomics *100*, 37–43.

Toyoshima, M., Tanaka, N., Aoki, J., Tanaka, Y., Murata, K., Kyuuma, M., Kobayashi, H., Ishii, N., Yaegashi, N., and Sugamura, K. (2007). Inhibition of tumor growth and metastasis by depletion of vesicular sorting protein Hrs: its regulatory role on E-cadherin and beta-catenin. Cancer Res. *67*, 5162–5171.

Urbé, S., Mills, I.G., Stenmark, H., Kitamura, N., and Clague, M.J. (2000). Endosomal localization and receptor dynamics determine tyrosine phosphorylation of hepatocyte growth factor-regulated tyrosine kinase substrate. Mol. Cell Biol. *20*, 7685–7692.

Vietri, M., Radulovic, M., and Stenmark, H. (2020). The many functions of ESCRTs. Nat. Rev. Mol.Cell Biol *21*, 25–42.

Wang, J., Tucholska, M., Knight, J.D., Lambert, J.-P., Tate, S., Larsen, B., Gingras, A.-C., and Bandeira, N. (2015). MSPLIT-DIA: sensitive peptide identification for data-independent acquisition. Nat. Methods *12*, 1106–1108.

Wang, T., Liu, N.S., Seet, L.F., and Hong, W. (2010). The emerging role of VHS domain-containing Tom1, Tom1L1 and Tom1L2 in membrane trafficking. Traffic *11*, 1119–1128.

Wegener, C.S., Malerød, L., Pedersen, N.M., Prodiga, C., Bakke, O., Stenmark, H., and Brech, A. (2010). Ultrastructural characterization of giant endosomes induced by GTPase-deficient Rab5. Histochem.Cel.Biol. *133*, 41.

Wegner, C.S., Rodahl, L.M., and Stenmark, H. (2011). ESCRT proteins and cell signalling. Traffic *12*, 1291–1297.

Wenzel, E.M., Schultz, S.W., Schink, K.O., Pedersen, N.M., Nähse, V., Carlson, A., Brech, A., Stenmark, H., and Raiborg, C. (2018). Concerted ESCRT and clathrin recruitment waves define the timing and morphology of intraluminal vesicle formation. Nat. Commun. *9*, 1–18.

Yamaguchi, H., Wyckoff, J., and Condeelis, J. (2005). Cell migration in tumors. Curr.Opin.Cel. Biol. *17*, 559–564.

Yamakami, M., Yoshimori, T., and Yokosawa, H. (2003). Tom1, a VHS domain-containing protein, interacts with tollip, ubiquitin, and clathrin. J. Biol. Chem. *278*, 52865–52872.

STAR★METHODS

KEY RESOURCES TABLE

REAGENT or RESOURCE	SOURCE	IDENTIFIER
Antibodies		
Endofin	Proteintech	13118-2-AP
HD-PTP	Proteintech	10472-1-AP
Myc-Tag	Cell Signaling	2276
Hrs	Proteintech	10390-1-AP
STAM	Proteintech	12434-1-AP
Tsg101	Proteintech	14497-1-AP
UBAP1	Proteintech	12385-1-AP
Vps37A	Proteintech	11870-1-AP
CHMP4B	Proteintech	13683-1-AP
EGFR (A-10) used for WB and IP	Santa Cruz	Sc-373746
EGFR (ICR10) used for cs-ELISA, IF and FRIA	Abcam	Ab231
Integrin a5 used for WB	Proteintech	10569-1-AP
Integrin a5 used for cs-ELISA and FRIA	BD Pharmingen	555651
Anti-Human integrin a5b1	Millipore	MAB1969
CD4 (H370) used for WB	Santa Cruz	Sc-7219
CD4 (OKT4) used for FRIA	Invitrogen	14-0048-82
Flag-Tag (M2)	Sigma	F1804
eEF2	Cell Signaling	2332
a-Tubulin	Sigma	T6074
Clathrin (X22)	Abcam	Ab2731
EEA1	Invitrogen	14-9114-82
anti-Rat HRP F(ab')2	Jackson ImmunoResearch	712-036-153
anti-Mouse HRP F(ab')2	Jackson ImmunoResearch	115-036-003
anti-Rat FITC F(ab')2	Jackson ImmunoResearch	712-096-150
anti-Mouse AF488	Invitrogen	A-28175
anti-Mouse AF594	Invitrogen	A-11032
anti-Rabbit AF488	Invitrogen	A-27034
anti-Rabbit AF594	Invitrogen	A-11012
anti-Rat AF647	Invitrogen	A-21247
Chemicals, peptides, and recombinant proteins		
Recombinant Human EGF	Gibco	PHG0311
Human Plasma Fibronectin	Gibco	33016-015
Cycloheximide	Sigma	66-81-9
Bafilomycin A1	Sigma	B1793
CCCP	Sigma	C2759
Monensin sodium	Sigma	M5273
Nigericin sodium salt	Sigma	N7143
Amplex Red	Invitrogen	A12222

(*Continued on next page*)

Continued

REAGENT or RESOURCE	SOURCE	IDENTIFIER
Deposited data		
AP-MS Data	https://massive.ucsd.edu/ProteoSAFe/static/massive.jsp	MassIVE: MSV00087704
BirA BioID MSPLIT Data	https://massive.ucsd.edu/ProteoSAFe/static/massive.jsp	MassIVE: MSV00087705
MiniTurbo BioID MSPLIT Data	https://massive.ucsd.edu/ProteoSAFe/static/massive.jsp	MassIVE: MSV00087706
Experimental models: cell lines		
HeLa NT	Pause Lab	
HeLa sh54Endofin	Pause Lab	
HeLa sh75Endofin	Pause Lab	
HeLa sh47HD-PTP	Pause Lab	
HeLa sh51HD-PTP	Pause Lab	
HeLa sh98Hrs	Pause Lab	
293T NT	Pause Lab	
293T sh54Endofin	Pause Lab	
293T sh75Endofin	Pause Lab	
293T sh47HD-PTP	Pause Lab	
Oligonucleotides		
Details of cloning and mutagenesis primers are in Table S1		
Recombinant DNA		
pcDNA3-Flag-Endofin	Pause Lab	
pcDNA3-Flag-Endofin resistant to shRNA54	Pause Lab	
pcDNA3-Flag-L15P-Endofin resistant to shRNA54	Pause Lab	
pcDNA3-Flag-C753S-Endofin resistant to shRNA54	Pause Lab	
pcDNA3-Flag-HD-PTP	Pause Lab	
pcDNA3-Flag-HD-PTP resistant to shRNA47	Pause Lab	
pcDNA3-Flag-T145K-HD-PTP resistant to shRNA47	Pause lab	
pcDNA3-CD4TI	Lukacs Lab	
pcDNA3-CD4TI-Ub	Lukacs Lab	
pcDNA3-CD4TCC-UbAIIRΔG	Lukacs Lab	
Software and algorithms		
MetaMorph/MetaFluor Software	Molecular Devices	
Origin Software	OriginLab	https://www.originlab.com/
ImageJ Software		https://imagej.nih.gov/ij/

RESOURCE AVAILABILITY

Lead contact

Further information and requests for resources and reagents should be directed to and will be fulfilled by the lead contact, Arnim Pause (arnim.pause@mcgill.ca).

Materials availability

Plasmids and cell lines generated in this study are available from the lead contact.

Data and code availability

- All proteomics data in this study have been deposited at https://massive.ucsd.edu/ProteoSAFe/static/massive.jsp and are publicly available as of the date of publication. Accession numbers are listed in the key resources table.
- This paper does not report original code.
- Any additional information required to reanalyze the data reported in this paper is available from the lead contact upon request.

EXPERIMENTAL MODEL AND SUBJECT DETAILS

Cell lines

Endofin- and HD-PTP-depleted HeLa and 293T cells were generated from wild-type cells purchased from ATCC. All cell lines generated in this study are listed in the key resources table and available from the lead contact upon request.

METHODS DETAILS

Constructs, reagents and cell culture

Myc-tagged Endofin was a kind gift from Dr. H. Wang (Seet and Hong, 2001). pcDNA3-Flag-Endofin was generated by PCR amplification using myc-Endofin as a template and subcloning into the pcDNA3-Flag vector. pcDNA3-Flag-Endofin resistant to shRNA54 was generated by mutagenesis to introduce silent point mutations in the region targeted by the shRNA. This construct was used to create the C753S and L15P Endofin mutants obtained from BioBasic. Flag-tagged HD-PTP in pcDNA3.1 was described previously by Gingras et al. (Gingras et al., 2009). pcDNA3-Flag-HD-PTP resistant to shRNA47 was generated by mutagenesis to introduce silent mutations in the shRNA targeted region. This construct was further mutated to obtain the T145K HD-PTP mutant (BioBasic). The FYVE-Tom1 chimera was generated in the pcDNA3-Flag vector by subcloning a tandem repeat of the coding region for Endofin FYVE domain followed by a linker and the coding sequence for Tom1 (Biomatik). pcDNA3-CD4 c-tail was replaced by a linker followed by either WT Ub (CD4Tl-Ub) or CC tetramerization domain with mutant Ub (all K to R and deletion of 76GG (CD4TCC-UbAllRΔG) as described by Barriere et al. (Barriere et al., 2006). pCS2-RFP-Hrs was a gift from Dr. E.M. De Robertis (Addgene plasmid #29685). pLNCX2-mCherry-CHMP4B was a gift from Dr. S. Simon (Addgene plasmid #116923). Complete list of primers is included in Table S1.

HeLa (ATCC® CCL-2™) and 293T (ATCC® CRL-3216™) cells were cultured in DMEM, 10% FBS (Wisent). MISSION® shRNA Lentiviral plasmids pLKO.1-puro for human Endofin (clone ID: NM_014733.2-4263s1c1 (sh54), NM_014733.3-3858s21c1 (sh75)), human HD-PTP (clone ID: NM_015466.x-571s1c1 (sh47), NM_015466.x-887s1c1 (sh51)), human Hrs (clone ID: NM_004712.3-494s1c1 (sh98)) and empty vector (MISSION® pLKO.1-puro Empty Vector Control Plasmid DNA, SHC001) were purchased from Sigma.

The complete list of antibodies used in this study are included in key resources table. Complementation experiments were performed *via* transient transfection using Lipofectamine 2000 (Invitrogen) according to manufacturer's instructions. Complete list of reagents used in this study are included in key resources table.

AP-MS cloning, stable cell line generation and sample collection

The ORFs were transferred via Gateway cloning into N-terminal 3XFLAG mammalian expression vector for isogenic stable cell line generation and tetracycline-inducible expression. Flip-In T-REx 293T cells were transfected in a 6 well format with 0.2μg of tagged DNA (pcDNA5-FLAG-protein) and 2μg pOG44 (OpenFreezer V4134), using lipofectamine 2000 (Invitrogen), according to manufacturer's instructions. On day 2, cells were trypsinized, and passaged into 10 cm plates. On day 3, the medium is replaced by DMEM 10% Fetal bovine serum, 100 units/ml pen/strep, 200 ug/ml hygromycin. Medium was replaced every 2–4 days until non-transfected cells die, and isolated clones were ~1–2 mm in diameter (13–15 days). Pools of cells were generated by trypsinization of the entire plate and replating in fresh selection medium (the size of the plate was dictated by the number and size of initial colonies). Cells at ~ 60–70% confluence were induced with 1 μg/ml tetracycline for 24 hours. Subconfluent cells (~85-95% confluent) were harvested for AP-MS analysis.

BioID cloning, stable cell line generation and sample collection

Constructs for Endofin and HD-PTP were cloned into 5′ BirA* pcDNA5-FRT-TO or pcDNA5-FRT-TO 3′ BirA*. Constructs for EGFR were cloned into 5′ (MiniTurbo pcDNA5-FRT-TO or pcDNA5-FRT-TO 3′ MiniTurbo. Flip-In T-REx 293T cells (Endofin-BirA* and HD-PTP-BirA*) or Flip-In T-Rex HeLa cells (EGFR-miniTurbo) were transfected in a 6 well format with 0.2μg of cloned constructs and 2μg pOG44 (OpenFreezer V4134), using lipofectamine 2000 (Invitrogen), according to manufacturer's instructions. On day 2, cells were trypsinized, and passaged into 10 cm plates. On day 3, the medium is replaced by DMEM 10% fetal bovine serum, 100 units/ml pen/strep, 200 ug/ml hygromycin. Medium was replaced every 2- 4 days until non-transfected cells die, and isolated clones were ∼1-2 mm in diameter (13-15 days). Pools of cells were generated by trypsinization of the entire plate and replating in fresh selection medium (the size of the plate was dictated by the number and size of initial colonies). For BirA* experiments, cells ∼ 60-70% confluence were induced with 1ug/ml tetracycline for 24 hours. The next day, tetracycline-containing medium was supplemented with 50 μM biotin and cells were incubated for an additional 24 hours. For EGFR-miniTurbo experiments, cells ∼ 60-70% confluence were induced with 1ug/ml tetracycline for 24 hours in biotin-depleted medium. On day 2, cells were switched to tetracycline-containing, serum-free medium. After 16 hours of serum starvation, the medium was supplemented with 50 μM biotin for 15 minutes in the presence or absence of 100ng/mL EGF. To harvest, cells were scraped off in ice-cold PBS, washed x2 in PBS, pelleted and frozen at −80°C until processing for MS.

AP-MS and BioID sample processing and mass spectrometry analysis

For AP-MS studies, FLAG affinity purifications were performed as described previously by St-Denis et al. (St-Denis et al., 2016) and $^1/_4$ of each sample was analyzed by Velos Orbitrap mass spectrometry. A spray tip was formed on fused silica capillary column (0.75 μm ID, 350 μm OD) using a laser puller (program = 4; heat = 280, FIL = 0, VEL = 18, DEL = 200). 10 cm (+/- 1 cm) of C18 reversed-phase material (Reprosil-Pur 120 C18-AQ, 3 μm) was packed in the column by pressure bomb (in MeOH). The column was then pre-equilibrated in buffer A (6 μl) before being connected in-line to a NanoLC-Ultra 2D plus HPLC system (Eksigent) coupled to a LTQ-Orbitrap Velos (Thermo Electron) equipped with a nanoelectrospray ion source (Proxeon Biosystems). The LTQ-Orbitrap Velos instrument under Xcalibur 2.0 was operated in the data dependent mode to automatically switch between MS and up to 10 subsequent MS/MS acquisitions. Buffer A was 100% H2O, 0.1% formic acid; buffer B was 100 ACN, 0.1% formic acid. The HPLC gradient program delivered an acetonitrile gradient over 125 min. For the first twenty minutes, the flow rate was 400 μL/min at 2% B. The flow rate was then reduced to 200 μL/min and the fraction of solvent B increased in a linear fashion to 35% until 95.5 min. Solvent B was then increased to 80% over 5 min and maintained at that level until 107 min. The mobile phase was then reduced to 2% B until the end of the run (125 min). The parameters for data dependent acquisition on the mass spectrometer were: 1 centroid MS (mass range 400–2000) followed by MS/MS on the 10 most abundant ions. General parameters were: activation type = CID, isolation width = 1 m/z, normalized collision energy = 35, activation Q = 0.25, activation time = 10 msec. For data dependent acquisition, the minimum threshold was 500, the repeat count = 1, repeat duration = 30 sec, exclusion size list = 500, exclusion duration = 30 sec, exclusion mass width (by mass) = low 0.03, high 0.03.

For BirA* BioID studies, streptavidin pulldowns were performed as described previously St-Denis et al. (St-Denis et al., 2016) and $^1/_4$ of each sample was run on a TripleTOF™ 5600 instrument (AB SCIEX, Concord, Ontario, Canada). Nano-spray emitters were generated from fused silica capillary tubing, with 75μm internal diameter, 365μm outer diameter and 5-8μm tip opening, using a laser puller (Sutter Instrument Co., model P-2000, with parameters set as heat: 280, FIL = 0, VEL = 18, DEL = 2000). Nano-spray emitters were packed with C18 reversed-phase material (Reprosil-Pur 120 C18-AQ, 3μm) resuspended in methanol using a pressure injection cell. Samples were directly loaded at 400nl/min for 14min onto a 75μmx10cm nano-spray emitter. Peptides were eluted from the column with an acetonitrile gradient generated by an Eksigent ekspert™ Nano Ultra 1D Plus and analyzed on the TripleTOF. The gradient was delivered at 200nl/min from 2% acetonitrile with 0.1% formic acid to 35% acetonitrile with 0.1% formic acid using a linear gradient of 90 min. This was followed by a 10 min wash with 80% acetonitrile with 0.1% formic acid, and equilibration for another 15min to 2% acetonitrile with 0.1% formic acid. The total DDA protocol was 140min. The first DDA scan had an accumulation time of 250ms within a mass range of 400-1250Da. This was followed by 20 MS/MS scans of the top 20 peptides identified in the first DDA scan, with accumulation time of 100 ms for each MS/MS scan. Each candidate ion was required to have a charge state from 2-4 and a

minimum threshold of 250 counts per second, isolated using a window of 50mDa. Previously analyzed candidate ions were dynamically excluded for 15 seconds.

For MiniTurbo BioID studies, streptavidin pulldowns were performed as described previously by Hesketh et al. (Hesketh et al., 2020) and 1/6 of each sample was run on a TripleTOF™ 6600 instrument (AB SCIEX, Concord, Ontario, Canada). Samples were directly loaded at 800 nL/min onto an equilibrated HPLC column and LC-MS/MS was performed on a tripleTOF instrument as previously reported by Hesketh et al. (Hesketh et al., 2020). Samples were analyzed with two separate injections with instrument methods set to data dependent acquisition (DDA) and data independent acquisition (SWATH) modes, as reported previously by Hesketh et al. (Hesketh et al., 2020).

Data-dependent and independent acquisition data searches

Data-dependent mass spectrometry data was stored, searched and analyzed using ProHits laboratory information management system (LIMS) platform. Within ProHits, WIFF files were converted to an MGF format using the WIFF2MGF converter and to an mzML format using ProteoWizard (V3.0.10702) and the AB SCIEX MS Data Converter (V1.3 beta). The data was then searched using Mascot (V2.3.02) and Comet (V2016.01 rev.2). The spectra were searched with the human and adenovirus sequences in the RefSeq database (version 57, January 30th, 2013) acquired from NCBI, supplemented with "common contaminants" from the Max Planck Institute (http://maxquant.org/contaminants.zip) and the Global Proteome Machine (GPM; ftp://ftp.thegpm.org/fasta/cRAP/crap.fasta), forward and reverse sequences (labeled "gi|9999" or "DECOY"), sequence tags (BirA, GST26, mCherry and GFP) and streptavidin, for a total of 72,481 entries. Database parameters were set to search for tryptic cleavages, allowing up to 2 missed cleavages sites per peptide with a mass tolerance of 35ppm for precursors with charges of 2+ to 4+ and a tolerance of 0.15amu for fragment ions. Variable modifications were selected for deamidated asparagine and glutamine and oxidized methionine. Results from each search engine were analyzed through TPP (the Trans-Proteomic Pipeline, v.4.7 POLAR VORTEX rev 1) via the iProphet pipeline.

MSPLIT-DIA SWATH MS data were analyzed using MSPLIT-DIA (version 1.0 (Wang et al., 2015)) implemented in ProHits 4.0 (Liu et al., 2016). To generate a sample-specific spectral library, peptide-spectrum matches (PSMs) from matched DDA runs (BirA*) were pooled by retaining only the spectrum with the best MS-GFDB (Beta version 1.0072 (6/30/2014) (Kim et al., 2010)) probability for each unique peptide sequence and precursor charge state. The MS-GFDB parameters were set to search for tryptic cleavages with a precursor mass tolerance of 50 ppm and charges of 2+ – 4+. Peptide length was limited to 8–30 amino acids and oxidized methionine selected as a variable modification. For MiniTurbo searches, the Human SWATH Atlas (Rosenberger et al., 2014) served as the search library. A peptide-level false discovery rate (FDR) of 1% was enforced using a targetdecoy approach (Elias and Gygi, 2007). The spectra were searched with the NCBI RefSeq database (version 57, January 30th, 2013) against a total of 7 36,241 human and adenovirus sequences supplemented with common contaminants from the Max Planck Institute (http://141.61.102.106:8080/share.cgi?ssid=0f2gfuB) and the Global Proteome Machine (GPM; http://www.thegpm.org/crap/index.html). The spectral library was then used for peptide spectral matching to proteins by MSPLIT with peptides identified by MSPLIT-DIA passing a 1% FDR subsequently matched to genes using ProHits 4.0 (Liu et al., 2016).

SAINT analysis by SAINTexpress (version 3.6.1 (Teo et al., 2014)) was used to score interactions for all data. For AP-MS results, bait runs (two biological replicates each) were compared against 8 negative controls (GFP-FLAG). For BirA*-MSPLIT results, bait runs (two biological replicates each) were compared against four negative control runs (BirA*-FLAG and BirA*FLAG-GFP). For MiniTurbo-MSPLIT results, bait runs (two biological replicates each) were compared against five negative control runs (GFP-FLAG-miniTurbo and FLAG-miniTurbo). Preys with a false discovery rate (FDR) $\leq$ 1% (Bayesian estimation based on distribution of the Averaged SAINT scores across biological replicates) were considered high-confidence proximity interactions and were presented using dot plots generated using ProHits-viz (Knight et al., 2017)) (prohitsviz.lunenfeld.ca). In ProHits-viz, once a prey passes the selected FDR threshold (here 1%) with at least one bait, all its quantitative values across the dataset are retrieved for all baits. Bait-prey proximity interactions falling below the 5% FDR threshold are indicated by the color of the edge.

Proteomics data deposition

AP-MS data has been deposited as a complete submission to the MassIVE repository (https://massive.ucsd.edu/ProteoSAFe/static/massive.jsp) and assigned the accession number MSV00087704. The

ProteomeXchange accession is PXD026937. The dataset is currently available to the public at ftp://massive.ucsd.edu/MSV000087704/.

BirA BioID MSPLIT data has been deposited as an incomplete submission to the MassIVE repository (https://massive.ucsd.edu/ProteoSAFe/static/massive.jsp) and assigned the accession number MSV00087705. The dataset is currently available to the public at ftp://massive.ucsd.edu/MSV000087705/.

MiniTurbo BioID MSPLIT data has been deposited as an incomplete submission to the MassIVE repository (https://massive.ucsd.edu/ProteoSAFe/static/massive.jsp) and assigned the accession number MSV00087706. The dataset is currently available to the public at ftp://massive.ucsd.edu/MSV000087706/.

STRING analysis

Protein-protein interaction networks were generated using the STRING database (Szklarczyk et al., 2019). Colored nodes represent the first shell of interactors identified from the BioID screen using a BFDR cutoff of 0.01 and SAINT score above 0.85. White nodes represent the second shell of interactors extracted from the STRING database. The edges represent protein-protein interactions collected from STRING experiments and databases. The thickness of the edge reflects its confidence score. A maximum of 50 proteins is represented in the second shell of interactors and unique interactors were removed from the network.

Immunoprecipitation

Cells were lysed on ice in buffer A (50 mM Tris pH 7.5, 50 mM NaCl, 1,5 mM $MgCl_2$, 1 mM EDTA, 0.2% triton x-100, 5% glycerol, 1 mM DTT and cOmplete (Roche) protease inhibitors). Protein extracts were spun at 16,000g for 10 min at 4°C. A fraction of the supernatant was kept for SDS-PAGE and Western blots. The remaining fraction was pre-cleared then incubated with the primary antibody under agitation for 1h at 4°C. Protein-antigen complexes were retrieved with sepharose (Millipore) or magnetic beads (BioRad) coupled to an equal amount of protein A/G. Protein extracts were incubated with the beads under agitation for 1h at 4°C. Beads were then washed 3 times and eluted with Laemmli buffer followed by boiling the samples for 10 min. The immunoprecipitated fractions and the lysates were analyzed by SDS-PAGE followed by Western blotting.

Size-exclusion chromatography fractionation

Cells were lysed in buffer (150mM NaCl, 0.1% NP40, 6.25mM TrisHCl ph8, 2mM EDTA, 0.1mM MgCl2, 1mM EGTA, Protease inhibitor cocktail) on ice. The lysate was centrifuged first at 16,000g for 10min, and then the supernatant was centrifuged at 100,000g for 1h. The supernatant was loaded on Superdex200 HPLC column and 0.3ml fractions were collected. Protein analysis was performed on collected fraction by SDS-PAGE followed by Western blot.

Isopycnic sucrose gradient cellular fractionation

293T cells were washed with PBS on ice, scraped in low volume of ice-cold PBS on ice. The cell pellet was resuspended in isotonic buffer (20mM Hepes pH7.5; 150mM NaCl; 1mM DTT and protease inhibitor cocktail) and the cells were progressively broken down by needle strokes (10 strokes with 25-gauge needle, followed by 20 strokes with 27-gauge needle). The lysate was spun at 400g to eliminate nuclei, and the cytosolic supernatant was loaded on 10-40% sucrose gradient, centrifuged 16 h at 100,000g in Beckman Ti-55 rotor. The fractions were collected (0.25 ml) and analysed by Western blotting using the indicated markers.

Cycloheximide chase

Cells were starved for 2 h in serum-free DMEM media and pretreated for 1 h with cycloheximide (CHX, Sigma) (10 μg/ml for HeLa cells, 100 μg/ml for 293T cells). As a negative control, cells were pretreated for 1 h in the presence of CHX with Bafilomycin A1 (Sigma) to block lysosomal acidification and thus suppressing receptor lysosomal degradation. Next, cells were stimulated with EGF (50 ng/ml, 2 and 4 h) or with fibronectin (10 μg/ml, 3 and 6 h) in the presence of CHX in 0.5% FBS DMEM media at 37°C. After chasing the receptors for the indicated time points, cells were lysed on ice and receptor levels were analyzed by Western blotting.

Cell surface measurements using cs-ELISA

Cell-surface ELISA-based assays were performed in live cells as described by Apaja et al. (Apaja et al., 2010). Briefly, cells were starved for 2 h in serum-free DMEM media, labeled with integrin α5 or EGFR

antibodies on ice, and detected with horseradish peroxidase (HRP)-conjugated secondary antibody (Jackson ImmunoResearch) and Amplex Red (Life Technologies). In HeLa cells, internalization was measured after 5 min of EGF stimulation (50 ng/ml) at 37°C. For receptor stability experiments at the plasma membrane, integrin α5 and EGFR were stimulated with fibronectin (10 μg/ml, 4 h) and EGF (50 ng/ml, 20 min), respectively.

Pulse chase experiments and immunofluorescence

HeLa cells were seeded on glass coverslips and starved for 2 h in 0.5% FBS DMEM. For EGFR internalization, cells were stimulated with EGF (50 ng/ml, 5 min, 37°C) in 0.5% FBS DMEM. Next, EGF was washed with PBS and fresh 0.5% FBS DMEM media was added to chase EGFR for the indicated time points at 37°C. HeLa cells were fixed with 4% paraformaldehyde for 15 min and permeabilized with 0.1% Triton X-100 for 10 min at room temperature. Cells were labeled with primary antibodies for 1 h at room temperature followed by labelling with fluorescent secondary antibodies (Molecular probes, Invitrogen) and mounted for imaging. Sequential image acquisition was done on LSM780 confocal microscope (Carl Zeiss MicroImaging, Inc), using the Plan-Apochromat 63x/NA 1.4 objective.

Complementation experiments and vesicular cargo tracking using FRIA

Methodology for cargo labelled vesicular pH determination in live cells using FRIA has been described in Kazan et al. and Barriere et al. (Barriere and Lukacs, 2008; Kazan et al., 2019). Integrin α5 and EGFR were labelled with primary antibody and fluorescein isothiocyanate (FITC)-conjugated secondary Fab (Jackson ImmunoResearch) on ice and chased for indicated times. Transiently expressed CD4-Ub or CD4tCC-UbAllRΔG were used as before by Apaja et al. (Apaja et al., 2010). For complementation experiments, HeLa cells, seeded in 6 well plates, were transiently co-transfected by Lipofectamine 2000 (Invitrogen) with 0.5 μg of Endofin or HD-PTP constructs along with 100 ng of mcherry construct. 24 h post-transfection cells were seeded on glass coverslips (1.5 mm thickness, Fisher Scientific) to perform FRIA. FITC-dextran (10 kDa, 50 μg/ml, Molecular Probes) was used as control for lysosomal delivery. Dextran was endocytosed for 1 h and chased for 2 h at 37°C. Zeiss Observer Z1 (Carl Zeiss MicroImaging) equipped with X-Cite 120Q system (Lumen Dynamics Group Inc.) and MetaFluor software (Molecular Devices) were used to measure fluorescence intensities.

HeLa cell migration assay

Migration assays were performed using xCELLigence system (ACEA Biosciences). 30,000 HeLa cells in serum-free DMEM media were allowed to migrate for 24 h towards 10% FBS medium serving as a chemoattractant. As a negative control, cells were treated with α5β1 integrin blocking antibody (10 μg/ml). Rate of cellular migration was analyzed by plotting for the slope of the real-time migration curve of each cell line tested.

Signaling experiment

HeLa cells were starved for 2 h before treatment with EGF (5 ng/ml) or fibronectin (10 μg/ml) for the indicated time points at 37°C. Cells were collected and lysed on ice in buffer B (50 mM Tris pH 7.5, 150 mM NaCl, 1,5 mM $MgCl_2$, 1 mM EDTA, 1% triton x-100, 5% glycerol, 20 mM NaF, 5 mM NaPPi, 1 mM Na_3VO_4, 2 mM imidazole, 175 μg/ml PMSF and cOmplete (Roche) protease inhibitors). Protein extracts were separated by SDS-PAGE and analyzed by Western blotting.

QUANTIFICATION AND STATISTICAL ANALYSIS

Western blots and immunofluorescence images were quantified using imageJ software. FRIA data was quantified using MetaFluor software, and pHv peaks were drawn and further analyzed using Origin software. Statistical analysis was performed using Microsoft Excel software. Significance was determined by paired two-tailed Student's t test, and data with p values: *<0.05, **<0.01 and ***<0.001 are considered to be significant.